www.nautilos-h2020.eu

Organisation CNR
Department ISTI

# Automatic image analysis tools

## Accompanying report

Date: 30/03/2022
Doc. Version: v1.0
10.5281/zenodo.7224729

This project has received funding from the European Union's Horizon 2020 research and innovation programme under grant agreement No. 101000825 (NAUTILOS). This output reflects only the author's view and the European Union cannot be held responsible for any use that may be made of the information contained therein.

**Document Control Information**

| Settings | Value |
|---|---|
| **Deliverable Title** | Automatic image analysis tools |
| **Work Package Title** | Data Management |
| **Deliverable number** | D8.9 |
| **Description** | This deliverable will consist of the implementation of image analysis tools based on methods and algorithms designed explicitly to perform different automatic classifications. These tools will be used and applied both on already available and acquired images during the project. An accompanying report describing the tools will be produced. |
| **Lead Beneficiary** | CNR-ISTI |
| **Lead Authors** | Gabriele Pieri, Marco Reggiannini, Oscar Papini |
| **Contributors** | |
| **Submitted by** | Gabriele Pieri |
| **Doc. Version (Revision number)** | 1.0 |
| **Sensitivity (Security):** | Public |
| **Date:** | 30/03/2022 |
| **Doi** | 10.5281/zenodo.7224729 |

**Document Approver(s) and Reviewer(s):**

NOTE: All Approvers are required. Records of each approver must be maintained. All Reviewers in the list are considered required unless explicitly listed as Optional.

| Name | Role | Action | Date |
|---|---|---|---|
| **Flavio Martins** | WP9 Leader | *Approve* | 29/03/22 |
| | | | |
| | | | |

**Document history:**

The Document Author is authorised to make the following types of changes to the document without requiring that the document be re-approved:

- Editorial, formatting, and spelling
- Clarification

To request a change to this document, contact the Document Author or Owner.

Changes to this document are summarised in the following table in reverse chronological order (latest version first).

| Revision | Date | Created by | Short Description of Changes |
|---|---|---|---|
| **V0** | 18/01/22 | Pieri, Reggiannini | First structure of the deliverable ready for Review Team 1. |

| | | | |
|---|---|---|---|
| **V0.1** | 28/02/22 | Pieri, Reggiannini, Papini | Final structure decided and first inputs. |
| **V0.2** | 15/03/22 | Pieri, Reggiannini, Papini | Intermediate version. |
| **V0.3** | 23/03/22 | Pieri, Reggiannini, Papini | Updated and pre-finalized version. |
| **V0.4** | 24/03/22 | Reggiannini | Further integration of content. |
| **V0.5** | 28/03/22 | Pieri, Reggiannini, Papini | Final version ready for review. |
| **V0.6** | 30/03/22 | Pieri | Version reviewed, one minor bug fixed. |

**Configuration Management: Document Location**

The latest version of this controlled document is stored in <location>.

| **Nature of the deliverable** | | |
|---|---|---|
| **R** | Report | |
| **DEC** | Websites, patents, filing, etc. | |
| **DEM** | Demonstrator | |
| **O** | Other | √ |

| **Dissemination level** | | |
|---|---|---|
| **PU** | Public | √ |
| **CO** | Confidential, only for members of the consortium (including the Commission Services) | |

## Acknowledgement

This report forms part of the deliverables from the NAUTILOS project which has received funding from the European Union's Horizon 2020 research and innovation programme under grant agreement No 101000825. The Community is not responsible for any use that might be made of the content of this publication.

NAUTILOS - New Approach to Underwater Technologies for Innovative, Low-cost Ocean observation is an H2020 project funded under the Future of Seas and Oceans Flagship Initiative, coordinated by the National Research Council of Italy (CNR, Consiglio Nazionale delle Ricerche). It brings together a group of 21 entities from 11 European countries with multidisciplinary expertise ranging from ocean instrumentation development and integration, ocean sensing and sampling instrumentation, data processing, modelling and control, operational oceanography and biology and ecosystems and biogeochemistry such, water and climate change science, technological marine applications and research infrastructures.

NAUTILOS will fill-in marine observation and modelling gaps for chemical, biological and deep ocean physics variables through the development of a new generation of cost-effective sensors and samplers, the integration of the aforementioned technologies within observing platforms and their deployment in large-scale demonstrations in European seas. The fundamental aim of the project will be to complement and expand current European observation tools and services, to obtain a collection of data at a much higher spatial resolution, temporal regularity and length than currently available at the European scale, and to further enable and democratise the monitoring of the marine environment to both traditional and non-traditional data users.

NAUTILOS is one of two projects included in the EU's efforts to support of the European Strategy for Plastics in a Circular Economy by supporting the demonstration of new and innovative technologies to measure the Essential Ocean Variables (EOV).

More information on the project can be found at: https://www.nautilos-h2020.eu/.

## Copyright

# TABLE OF CONTENTS

**ACKNOWLEDGEMENT** ..... **4**

**COPYRIGHT** ..... **4**

**TABLE OF CONTENTS** ..... **5**

**EXECUTIVE SUMMARY** ..... **6**

**LIST OF FIGURES** ..... **7**

**LIST OF ACRONYMS AND ABBREVIATIONS** ..... **8**

**I. INTRODUCTION: TASK OBJECTIVES AND DELIVERABLE OUTLINE** ..... **9**

**II. ENVIRONMENTAL DOMAINS AND IMAGERY TYPOLOGIES** ..... **9**

1. Remote sensing scenario ..... 9
2. Close range sensing scenario ..... 10

**III. STATE OF THE ART OF AUTOMATIC IMAGE ANALYSIS ALGORITHMS** ..... **11**

1. Sea Surface Temperature pattern classification ..... 11
2. Benthic imagery classification ..... 13
   - 2.1. Segmentation through unsupervised techniques ..... 13
   - 2.2. Segmentation through semisupervised techniques ..... 14
3. Seafloor fauna detection ..... 15

**IV. DEVELOPED ALGORITHMS** ..... **16**

1. Sea Surface Temperature pattern classification ..... 16
   - 1.1. Plot SST values against time ..... 16
   - 1.2. Custom Python classes for SST data management ..... 19
   - 1.3. Mobile windows ..... 20
   - 1.4. Statistics analysis and classification ..... 22
2. Benthic imagery classification ..... 27
   - 2.1. Clustering pixel intensities ..... 28
   - 2.2. Clustering image features ..... 32
3. Seafloor fauna detection and counting ..... 33
   - 3.1. Background and requirements ..... 33
   - 3.2. The algorithm and the GUI ..... 36

**V. CONCLUSIONS** ..... **42**

**VI. BIBLIOGRAPHY** ..... **43**

**VII. APPENDIX 1: REFERENCES AND RELATED DOCUMENTS** ..... **45**

# EXECUTIVE SUMMARY

This deliverable is the concluding document, representing an accompanying report for the automatic image tools designed and developed as the main activity of Task 8.5 of Work Package 8 in NAUTILOS. As foreseen, the report describes the various steps performed within Task 8.5, starting from the definition of a set of various problems to be tackled, in close connections with end-users or experts partners within NAUTILOS; and then, moving to the collection and analysis of various imagery datasets to be used in the process; finally the developments of various automatic image analysis algorithms, on the basis of collected requirements and constraints is described. Different types of categorization or classification are required by each diverse environmental domain tool. Outcomes of this Task will be refined and improved within Task 9.5 in Work Package 9 through continuous feedbacks from experts and end-users, also exploiting the first testing and demonstration activities in NAUTILOS.

## LIST OF FIGURES

Figure 1. Examples of patterns identified in SST maps........................................................................12
Figure 2. Main window of the SST plot GUI..........................................................................................16
Figure 3. Example of a spaghetti plot (right). The SST map on the left is relative to a type 3 event identified on 19th September 2017 at 22:13 UTC (corresponding to the red vertical line in the plot on the right). On the top left: detail of the target area for the spaghetti plot (in this case [36.5° N, 37° N]×[9.5° W, 9° W] with a resolution of 0.05°) and reference grid, with each square corresponding to the graph with the same colour in the spaghetti plot.........................................................................17
Figure 4. SST annual trend for 2017 in the window [36° N, 37° N]×[10° W, 9° W]. The blue dots represent the average SST in the window; the red line is the interpolated curve. In this case $A = -2.564578038371188$, $\phi = 0.9652411407664284$, $\mu = 18.242557839045013$. .....................18
Figure 5. Spaghetti plots relative to the same area as Figure 4 and the same period of time. On the left: no adjustment is applied; on the right: values are modified according to the assumed annual SST trend. ........................................................................................................................................18
Figure 6. Top: example of spaghetti plot before the regularization; bottom: the same spaghetti plot after regularization, on the left with mode "discard" and on the right with mode "replace". ............20
Figure 7. Example of spaghetti plots produced with the mobile window tool. In this case a 0.5°×0.5° window has been selected, with a resolution of 0.125° and a stride of 0.25°. ..................................21
Figure 8. Visual representation of the statistics for SpaghettiData objects in the area of interest, in the period of 15 days from 1st to 15th September 2016, with SpaghettiData objects with resolution 0.25°. The expected number of data is two SST values per day (i.e. 30 values in a 15-day period), and SpaghettiData objects with less than 5 values are discarded. ...........................................................23
Figure 9. Scores for the squares computed according to the values of the statistics in Figure 7. .......26
Figure 10. Heatmap obtained from the scores of Figure 10. The tool finds a prevalent E3 event along the coast and traces of E1 and E2 events..........................................................................................27
Figure 11. HCMR Dataset examples: (a) coral; (b) macroalga; (c) seagrass; (d) seastar; (e) mollusc; (f) sponge. ...........................................................................................................................................27
Figure 12. Input image example (a) and the related RGB channels (b)-(d). .......................................29
Figure 13. CIE Lab representation: (a) brightness channel L; (b) chromaticity channel a*; (c) chromaticity channel b*. ....................................................................................................................29
Figure 14. K-means clustering with two classes applied to an HCMR image. (a) binarized image with cluster labels; (b) cluster I; (c) cluster II...............................................................................................30
Figure 15. K-means clustering with three classes applied to an HCMR image. (a) binarized image with cluster labels; (b) cluster I; (c) cluster II; (d) cluster III.........................................................................30
Figure 16. Orange sponge specimen (HCMR dataset)..........................................................................31
Figure 17. K-means clustering with two classes applied to an HCMR image of a sponge. (a) binarized image with cluster labels; (b) cluster I; (c) cluster II. ...........................................................................31
Figure 18. K-means clustering with three classes applied to an HCMR image of a sponge. (a) binarized image with cluster labels; (b) cluster I; (c) cluster II; (d) cluster III. ......................................................32
Figure 19. K-means clustering (two classes) of Gabor features applied to an erect dendritic sponge image: (a) input image; (b) cluster I; (c) cluster II.....................................................................................32
Figure 20. Screeshot from a video acquired for the nephrops burrows detection campaigns. ...........34
Figure 21. Significative signatures of a Nephrops burrow system. .....................................................35
Figure 22. The Graphical User Interface developed for the Nephrops burrow detection tool. ...........36
Figure 23. Loaded video file from GUI, showing first original frame...................................................37
Figure 24. Example of an original frame of the video (left) and after pre-processing (right). .............37
Figure 25. Flow diagram of the Nephrops burrow algorithm...............................................................38
Figure 26. Initial processing results before filtering. ...........................................................................38
Figure 27. Detection and identification of holes (red circles) and the structure (highlighted green rectangle) composed by these holes; the holes in white circles are identified as candidate holes but dismissed and not associated with the structure....................................................................39

Figure 28. Detection and identification of holes and structure (red circles, yellow rectangle) composed by these holes; the detected area in the white circle is dismissed and not associated with the structure. ....40
Figure 29. Highlight of the holes (lower yellow circle) and structures (upper yellow-circle) optical flows between the current frame and previous one. ....40
Figure 30. Example of multiple structures (2) detected. ....41
Figure 31. Another example with three different structures identified. ....41
Figure 32. Example of multiple and overlapping structures identified. ....42

## List of Acronyms and Abbreviations

| Abbreviation | Definition |
|---|---|
| **CS** | Citizen Science |
| **SST** | Sea Surface Temperature |
| **AVHRR** | Advanced Very High Resolution Radiometer |
| **MODIS** | Moderate Resolution Imaging Spectroradiometer |
| **SRM** | Statistical Region Merging |
| **ICES** | International Council for the Exploration of the Sea |
| **WGNEPS** | Working Group on Nephrops Surveys |
| **GUI** | Graphical User Interface |

# I. Introduction: task objectives and deliverable outline

This document represents an accompanying report to all the tools developed in the context of Task 8.5 of NAUTILOS. The idea behind this task was to provide tools for the automatic processing of some of the many different types of imagery data available among the different partners in the project. The first, very important step was to define with different partners the relevant domains where some type of processing could be studied and brought towards an automatic analysis. In addition, a search was carried out for available images, both from the same partners and in open access repositories.

Since the proposal stage, some of these tasks were already defined, while others raised from the various partners who needed support in the analysis phase of some of the tasks they have been facing. As an example, the categorisation of benthic imagery was already an open problem which was identified to be faced since the beginning, as it was also possibly connected with the Citizen Science (CS) activities (e.g. images acquired by divers).

Among any other type of problems, two different types of analysis raised from the partners within NAUTILOS. The first was pertaining the analysis of satellite imageries, with a particular reference to the Sea Surface Temperatures (SST), as being central to the analysis of an environmental problem concerning the identification of upwelling regimes.

The other type of analysis raised by another NAUTILOS partner, was concerning the detection and counting of seafloor fauna. In particular, the focus is on a specific marine fauna species, in order to detect and count the burrows constructed on the seafloor by *Nephrops norvegicus*, a seafloor resident species of crustacean lobster often called “scampi”.

The report is arranged as follows: the following section **Errore. L'origine riferimento non è stata trovata.** reports a description of the various different scenarios where data acquisition takes place and the specifics of the adopted sensing technologies; section III concerns a summary of the available methods found in the dedicated literature while the actually implemented algorithms are discussed in section IV; section V summarises the report providing conclusive discussions.

# II. Environmental domains and imagery typologies

In this section, a brief description of the distinctive features of each different scenario is given along with the specifics of the various imagery sets collected and analysed for this task.

## 1. Remote sensing scenario

The identification and classification of upwelling features in a marine ecosystem has been performed by experts by looking at SST maps of the area of interest. These maps are compiled using data coming from satellite missions; the same data have been used as input in the automatic classification tool described in section IV, subsection **Errore. L'origine riferimento non è stata trovata.** below.

For the SST analysis, satellite data from 2009 to 2017 has been retrieved from two different sources: EUMETSAT’s *Metop* programme [1] and NASA’s *Aqua* satellite [2]; they will be referred to respectively as “Metop dataset” and “Aqua dataset” hereafter.

The Metop dataset contains data gathered from the Advanced Very High Resolution Radiometer (AVHRR) of either Metop-A (2009–2016 data) or Metop-B (2017 data) satellites, processed at level L2P and binned in a single netCDF-4 file every 3 minutes, for a total of 480 images per day covering the entire globe, with a spatial resolution of 1 km at nadir and a temperature resolution of 0.01 °C.

The Aqua dataset contains data gathered from the Moderate Resolution Imaging Spectroradiometer (MODIS), processed at level L2P and binned in a single netCDF-4 file every 5 minutes, for a total of 288 images per day covering the entire globe, with a spatial resolution of 1 km at nadir and a temperature resolution of 0.005 °C.

In both cases, for each recorded SST value, the files store additional information, such as the latitude/longitude, the exact time of detection and a series of geophysical and navigational metadata. Moreover, a quality level is assigned to each value, meaning that it is possible for the end user to estimate the reliability of the data.

Both datasets can be openly accessed from the respective institution's websites; only files that contain data within the area of interest were downloaded.

## 2. CLOSE RANGE SENSING SCENARIO

Acoustic and optical sensing represent the most effective sensing technologies in the underwater environment. Concerning the observation and survey of marine underwater biological habitats, optical sensing is the first choice technology in the specific NAUTILOS frame.

The choice for the optical sensor class is also motivated by the need for the underwater scene survey task to be integrated and enriched with the citizen science involvement, whose typical sensing equipment consists of commercial off-the-shelf low cost devices, usually not developed for environmental mapping tasks carried out in hostile and complex frameworks, such as the underwater one. In this sense, optical sensors represent a proper trade off between the requirement of surveying a given underwater scenario with sufficient accuracy, either in terms of morphology and geometry representation as well as for its color information, and the need to choose largely diffused low cost devices in order to engage the largest possible portion of citizenry. Data collected by optical sensors operating in the visible band, find fruitful exploitation in biological marine tasks concerning marine fauna census or health status assessment of marine habitats. These two case studies have both been covered in NAUTILOS, adopting the approaches discussed in the following.

In NAUTILOS the mentioned optical cameras are exploited to capture high resolution images of a marine scene in order to perform flora population monitoring and safeguarding within predefined marine areas. For this purposes images' quality is usually high in terms of pixel resolution and color representation, so as to ensure the informative content in the scene is properly captured. The captured images can then be fed to classification algorithms aiming at a categorisation of each pixel.

Optical sensors are also exploited to perform specimen counting dedicated to specific fauna species, as in the case of *Nephrops norvegicus* (in the following Nephrops) burrows counting, a biological marine topic with large relevance both from a commercial point of view as well as for research purposes. Nephrops species population is usually assessed by means of a seafloor sledge, equipped with optical cameras downward and slanted looking. A surface vessel controls the sledge trajectory through a cable connection, which also allows to transfer the acquired videos. The goal is to perform a counting of the nephrops burrows that intercept the field of view of the camera, in order to later extrapolate a general statistics of the population numerosity. The standard methodology involves acquisitions filmed on the seabed at a grid of stations conducting TV tows for 10 minutes. Each country in Europe has adopted different sampling designs, from random stratifications of the stations up to fix grids, which better fits the grounds.

Both the mentioned topics will be further discussed in the following sections.

# III. STATE OF THE ART OF AUTOMATIC IMAGE ANALYSIS ALGORITHMS

In this section a brief report about the existing literature devoted to each of the above mentioned topics is provided. The main subdivision follows the path of the different algorithms developed in the activities of Task 8.5: firstly the SST analysis looking to identify temperature patterns, then the benthic imagery classification, and lastly, reaching the seabed, the seafloor fauna detection problem.

## 1. Sea Surface Temperature pattern classification

In the marine environment, the upwelling is the phenomenon of the upward vertical transport of cold, nutrient-rich water, mainly due to the action of winds and the Earth rotation. Upwelling ecosystems are among the most productive ones in the global ocean [3]; in fact, despite covering about 1% of the global sea surface, they account for 7% of the total marine production and more than 20% of the global fish catches. Understanding the behaviour of an upwelling ecosystem means not only to be able to study the effects of climate change in such environments, which are still under investigation [4], but also to develop appropriate and effective countermeasures for the preservation of the ecosystem in case of accidents (e.g. oil spills [5]).

*In this context, the identification of mesoscale upwelling events plays a central role. Historically this task has been performed by experts by looking at the SST maps, compiled from satellite data. As part of Task 8.5 of NAUTILOS, the analysis focused on the Iberia/Canary Current System, which is one of the most interesting and less studied upwelling ecosystem [6]; in particular, in the area near the south-western coast of the Iberian Peninsula (latitude between 35° N and 40° N, longitude between 12° W and 6° W), four patterns of SST linked to upwelling events have been identified (see*

The provided annotation consists of a Microsoft® Excel table with one row per second, linked with the observation note (e.g. “1 system left-centre + 1 collapsed right”), and the burrow count for that second, i.e. how many burrow systems in that second.

Following the extensive studies, since the early 2010s, in the ICES Working Group, the definition and characterising “signatures” of the Nephrops burrows have been outlined. For instance the appearance, the shape, and other significative features have been identified; in the following Figure 21 a sample of these is shown.

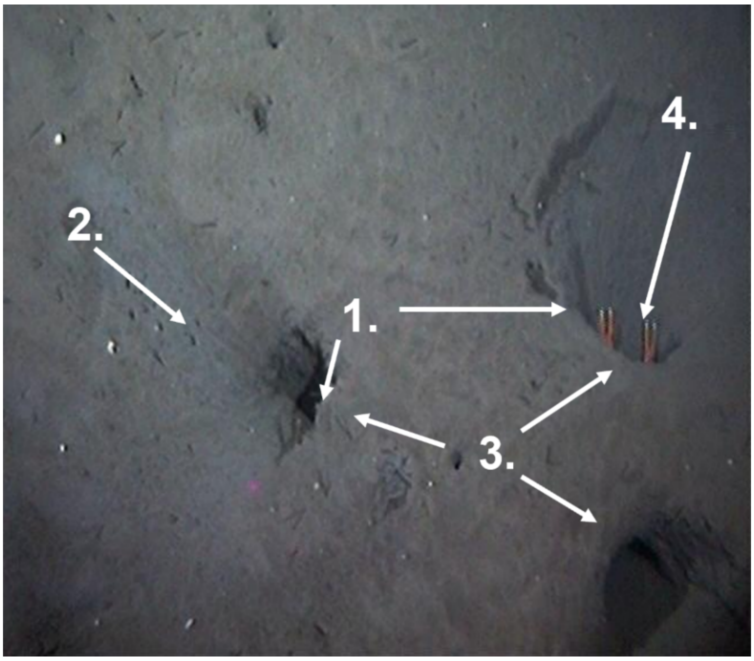

*Figure 21. Significative signatures of a Nephrops burrow system.*

In the figure, the numbered areas show the following features:

1. Crescentiform entrance of the burrow;
2. Sediment ejecta and radial scrapings around the entrance. Claw or pereiopod indents. “Drive-way”
3. Single to multiple entrances, focusing on an apparent “raised” centrum
4. Nephrops presence

Moreover, some high-level guidelines have been suggested to allow for a more standardised classification by the various ICES Working Groups experiences . These guidelines were helpful in the design of the algorithm to develop a method that was as close as possible to the procedures followed by the experts in their manual (i.e. visual) efforts. The main guidelines are as follows:

- Only count systems or parts of a system that cross an imaginary line just off the bottom of the screen.
- Include an entrance to a burrow if part of the shadow is still within sight as it crosses the line.
- Look for groups of similarly sized entrances radiating from a centrum, then look for Nephrops’ signatures.
- In poor visibility conditions, distinguishing the signatures will be more challenging; due to the low contrast, hemispherical entrances may appear as dark circular entrances. The signatures will appear less clear, but the ejected sediments and the disposition of the inlets will be the primary indicators.
- In the absence of Nephrops signatures, dismiss:
    - vertical holes;
    - flat holes with curved scrapings, sediment stacked in mounds.
- If in doubt, leave it out.

- Distance covered whilst the view is obscured by cloud and lifting needs to be discounted.
- Count and record in seconds, only for the period the sledge is moving.

### 1.1. The algorithm and the GUI

Following this and the meetings with experts who manually and visually classify the video, a tool based on developed algorithms and usable through a graphical user interface (GUI) has been designed to visualise better and test the automatic burrow detection tool. In the following Figure 22, the GUI is shown upon its loading.

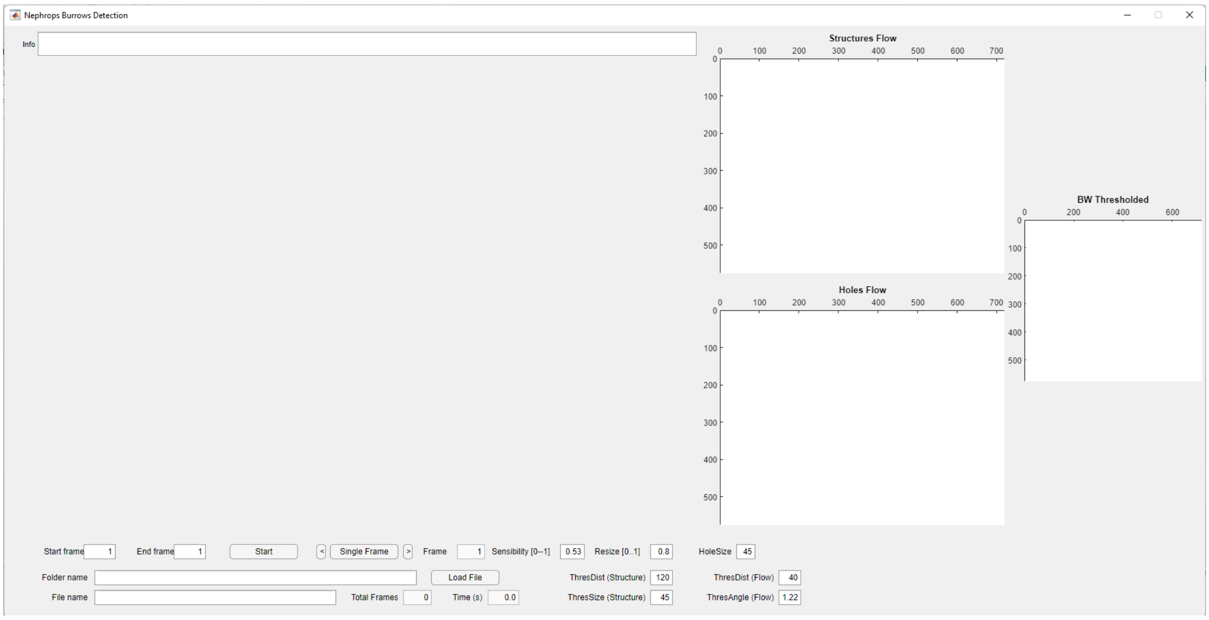

Start frame 1
End frame 1
Frame 1
Sensibility [0--1] 0.53
Resize [0..1] 0.8
HoleSize 45
Folder name
ThresDist (Structure) 120
ThresDist (Flow) 40
File name
Total Frames 0
Time (s) 0.0
ThresSize (Structure) 45
ThresAngle (Flow) 1.22

*Figure 22. The Graphical User Interface developed for the Nephrops burrow detection tool.*

The GUI is divided into three main areas: the left-centre panel will be filled by the images to be processed; in the centre-right and right panels, the graphs showing information will be represented; while the bottom part of the interface contains the buttons and fields used for controlling the tool (e.g. the button for loading a video file, for automatically processing a range of frames, for processing a single frame or the next one…), for viewing the video/frame information (e.g. video length, current frame number and time within the video…), as well as for setting the processing parameters (e.g. sensibility of the processing filters, the minimum size of holes, tracking and thresholding parameters for the geometries).

The first step to perform is selecting and loading the video to be analysed. An apparent problem can be seen as soon as the video is loaded due to the interlaced video acquired from TV recording (Figure 23). Thus, the first preprocessing step was to remove this interlacement and improve the single frame appearance. The difference can be seen in the following Figure 24 from the same frame after being loaded (left), and once it has been preprocessed, and ready for the beginning of processing (right).

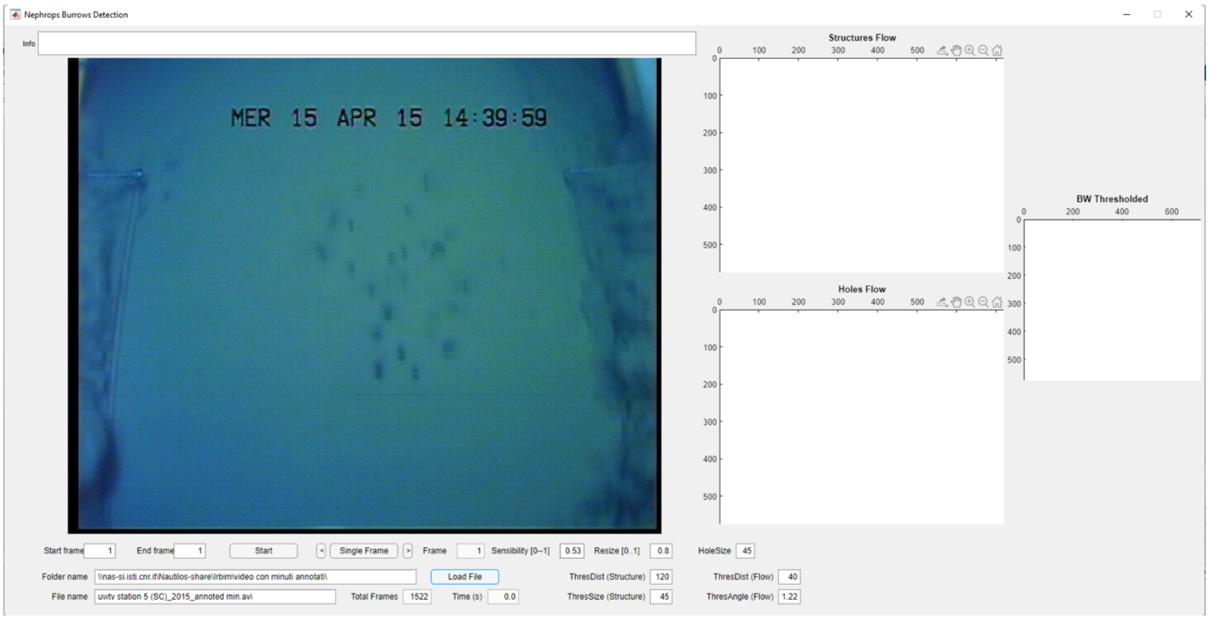

Start frame 1 End frame 1 Frame 1 Sensibility [0--1] 0.53 Resize [0..1] 0.8 HoleSize 45

Folder name \\nas-si.isti.cnr.it\Nautilos-share\Irbim\video con minuti annotati\ ThresDist (Structure) 120 ThresDist (Flow) 40

File name uwtv station 5 (SC)_2015_annoted min.avi Total Frames 1522 Time (s) 0.0 ThresSize (Structure) 45 ThresAngle (Flow) 1.22

*Figure 23. Loaded video file from GUI, showing first original frame.*

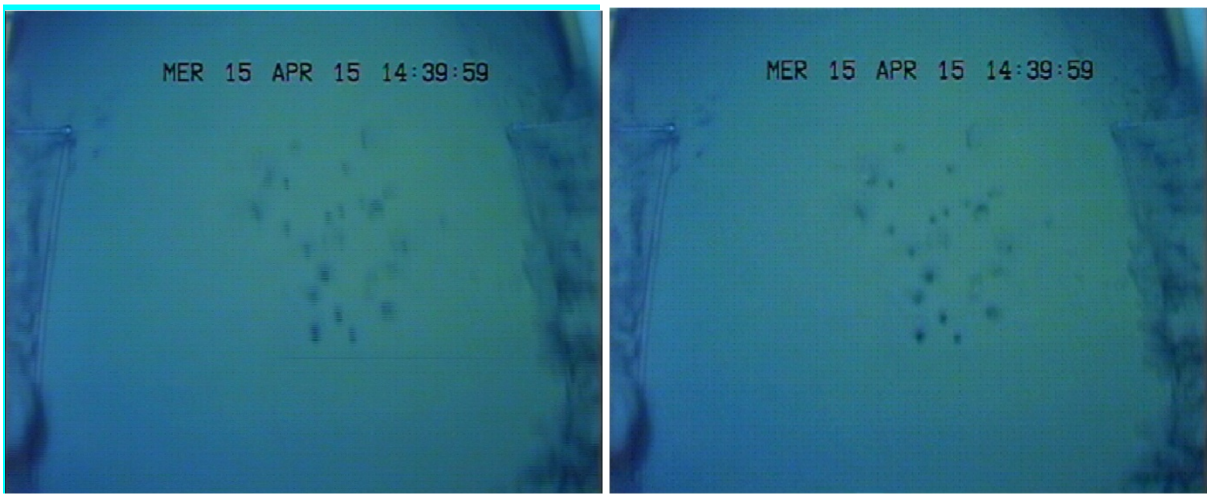

*Figure 24. Example of an original frame of the video (left) and after pre-processing (right).*

The general processing steps foresee two different analysis phases: only for the first frame the holes identification and selection, followed by the analysis and identification of the structures; on the subsequent frames, these first steps are repeated, but then the optical flow is used to understand and create connections between the identified holes and mainly among the identified structures. The processing flow diagram is shown in Figure 25.

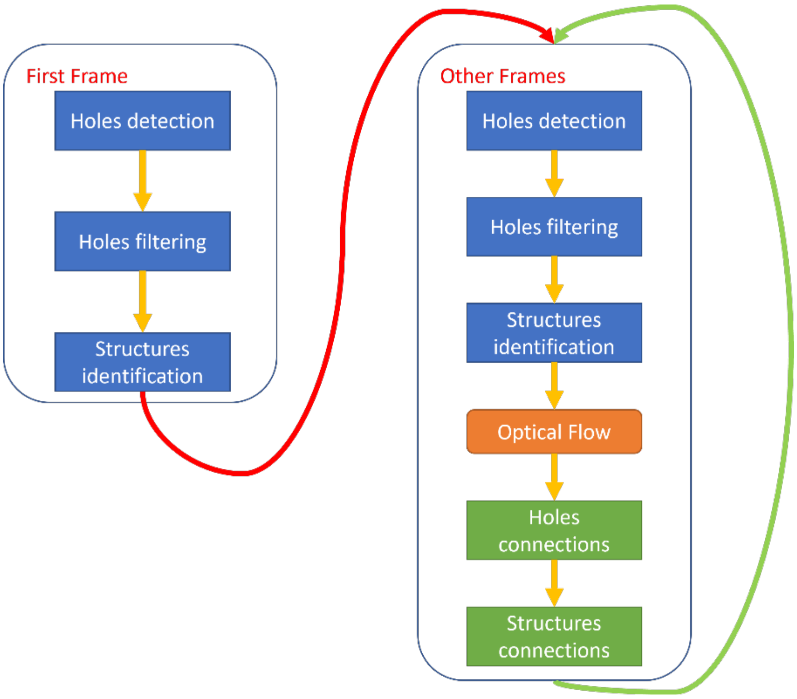

*Figure 25. Flow diagram of the Nephrops burrow algorithm.*

As a first processing step, holes are recognised through the identification of connected regions in the negative image using adaptive thresholding. The result of this processing is shown in the rightmost panel (blue/yellow coloured graph) of the GUI (see Figure 26).

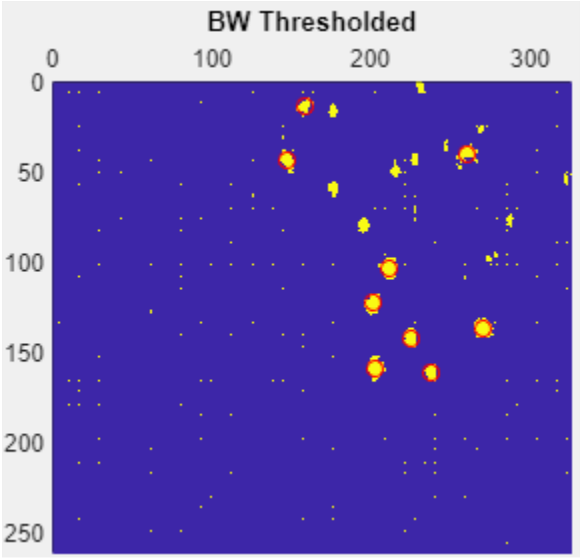

*Figure 26. Initial processing results before filtering.*

Subsequent processing steps filter over the detected holes to dismiss those below thresholds for dimension, shape, or position. Moreover, a colour histogram detects possible shadows and rejects them from the potential holes. Once the number of candidate holes is reduced, the geometric features are computed to analyse the shapes further. Features like: area, perimeter, the major axis of the area, eccentricity and circularity are extracted as well as the bounding box of each candidate hole.

Based on these parameters, rules have been defined for evaluating proximity, shape consistency, distances among holes and similarity by other geometric features. Based on these factors, structures composing a burrow system are identified. In the following Figure 27 the detection and identification of a structure, identified with its bounding box (green rectangle) and its composing holes (inside the red circles) are highlighted.

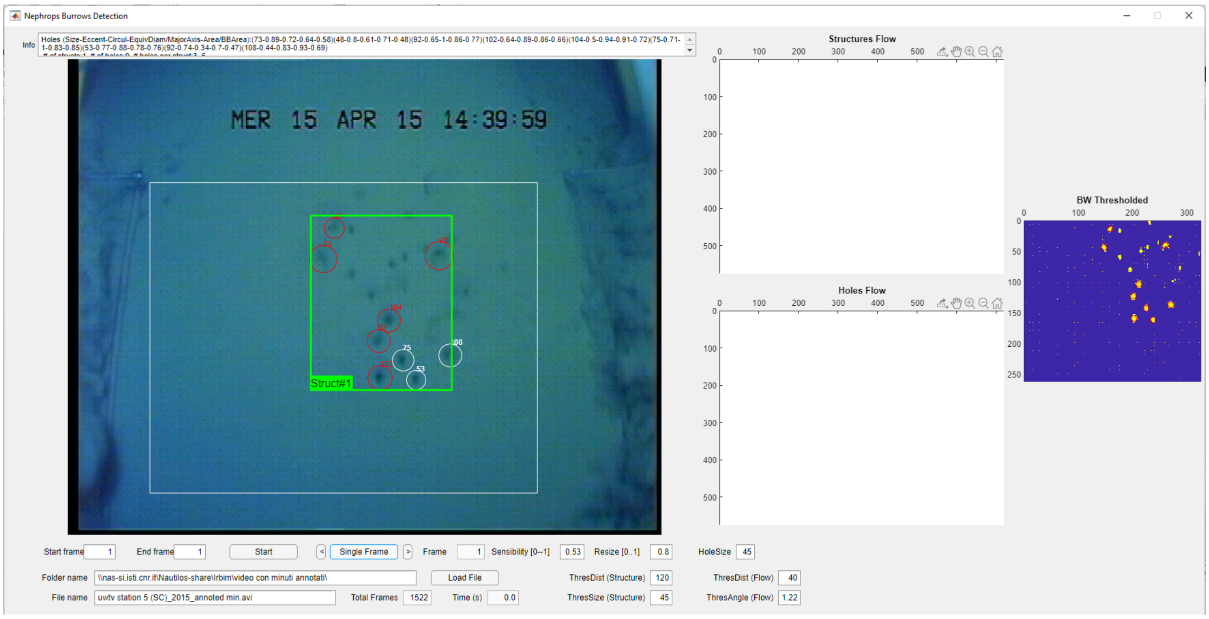

Nephrops Burrows Detection

Info: Holes (Size-Eccent-Circul-EquivDiam/MajorAxis-Area/BBArea):(73-0.89-0.72-0.64-0.58)(48-0.8-0.61-0.71-0.48)(92-0.65-1-0.86-0.77)(102-0.64-0.89-0.86-0.66)(104-0.5-0.94-0.91-0.72)(75-0.71-1-0.83-0.85)(53-0.77-0.88-0.78-0.76)(92-0.74-0.34-0.7-0.47)(108-0.44-0.83-0.93-0.69)
# of structs:1 # of holes:9 # holes per struct:3 6

Start frame 1 | End frame 1 | Start | < | Single Frame | > | Frame 1 | Sensibility [0--1] 0.53 | Resize [0..1] 0.8 | HoleSize 45

Folder name \\nas-si.isti.cnr.it\Nautilos-share\Irbim\video con minuti annotati\ | Load File | ThresDist (Structure) 120 | ThresDist (Flow) 40

File name uwtv station 5 (SC)_2015_annoted min.avi | Total Frames 1522 | Time (s) 0.0 | ThresSize (Structure) 45 | ThresAngle (Flow) 1.22

*Figure 27. Detection and identification of holes (red circles) and the structure (highlighted green rectangle) composed by these holes; the holes in white circles are identified as candidate holes but dismissed and not associated with the structure.*

The figure also shows some holes (in white circles) that have been identified as candidate holes but then filtered and discarded from the identified structure, due to a missing correspondence to the structure's geometric and appearance parameters.

Another example of filtered areas is shown in the following Figure 28; here, the noise brought in the video by the cloud of sand caused by the movement of the sledge on the left side is identified and easily filtered out as a false alarm and highlighted in the large white circle. The small numbers next to the circles represent the dimension of the identified connected areas, regardless of whether they belong to a structure. Furthermore, the text box above the processing frame shows statistics and information about the holes and structures identified in the current frame.

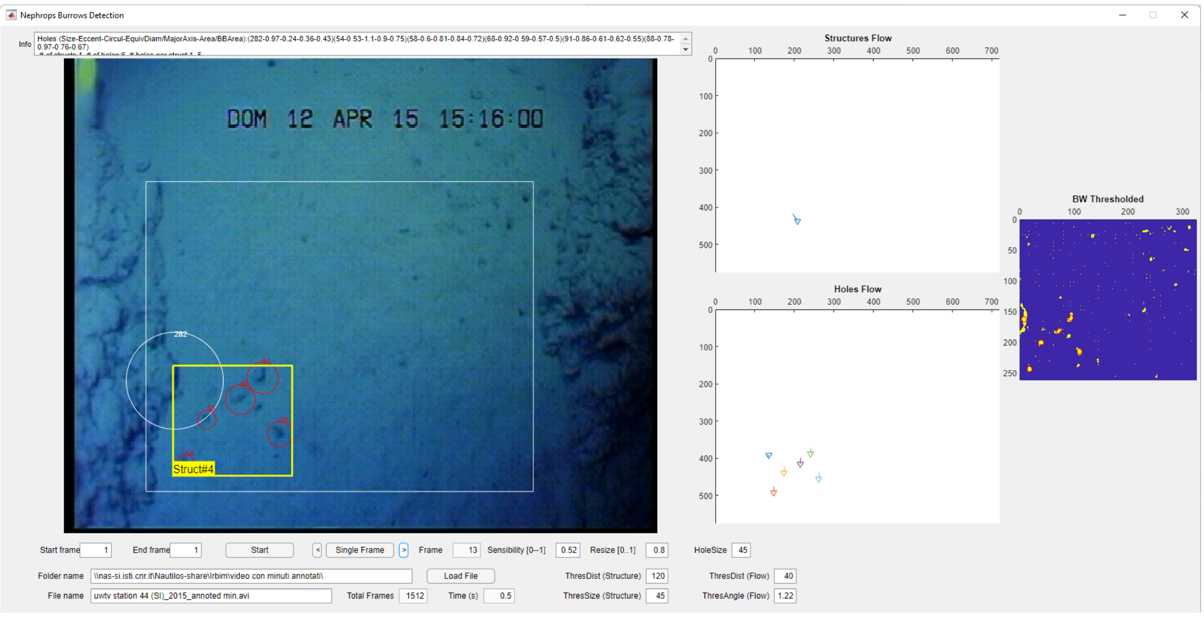

Nephrops Burrows Detection

Info: Holes (Size-Eccent-Circul-EquivDiam/MajorAxis-Area/BBArea):(282-0.97-0.24-0.36-0.43)(54-0.53-1.1-0.9-0.75)(58-0.6-0.81-0.84-0.72)(68-0.92-0.59-0.57-0.5)(91-0.86-0.61-0.62-0.55)(88-0.78-0.97-0.76-0.67)
# of structs:1, # of holes:6, # holes per struct:1, 5

Start frame 1 | End frame 1 | Start | < | Single Frame | > | Frame 13 | Sensibility [0--1] 0.52 | Resize [0..1] 0.8 | HoleSize 45

Folder name \\nas-si.isti.cnr.it\Nautilos-share\Irbim\video con minuti annotati\ | Load File | ThresDist (Structure) 120 | ThresDist (Flow) 40

File name uwtv station 44 (SI)_2015_annoted min.avi | Total Frames 1512 | Time (s) 0.5 | ThresSize (Structure) 45 | ThresAngle (Flow) 1.22

*Figure 28. Detection and identification of holes and structure (red circles, yellow rectangle) composed by these holes; the detected area in the white circle is dismissed and not associated with the structure.*

The next step, applied to all subsequent frames of the video, consists of the same detection and filtering steps as mentioned above, followed by an optical flow computation between the current frame structures and holes and the previous frame ones.

These optical flows are computed and then filtered, considering the known motion of the sledge and the geometric features of both the holes and structures. The optical flows are shown in the GUI central-right graphs (see Figure 29). A confusion matrix is computed associating holes/structures in frame $i$ and in frame $i-1$. This matrix is also important to understand whether a structure is persistent in subsequent frames or changed so that it should be identified as a new structure.

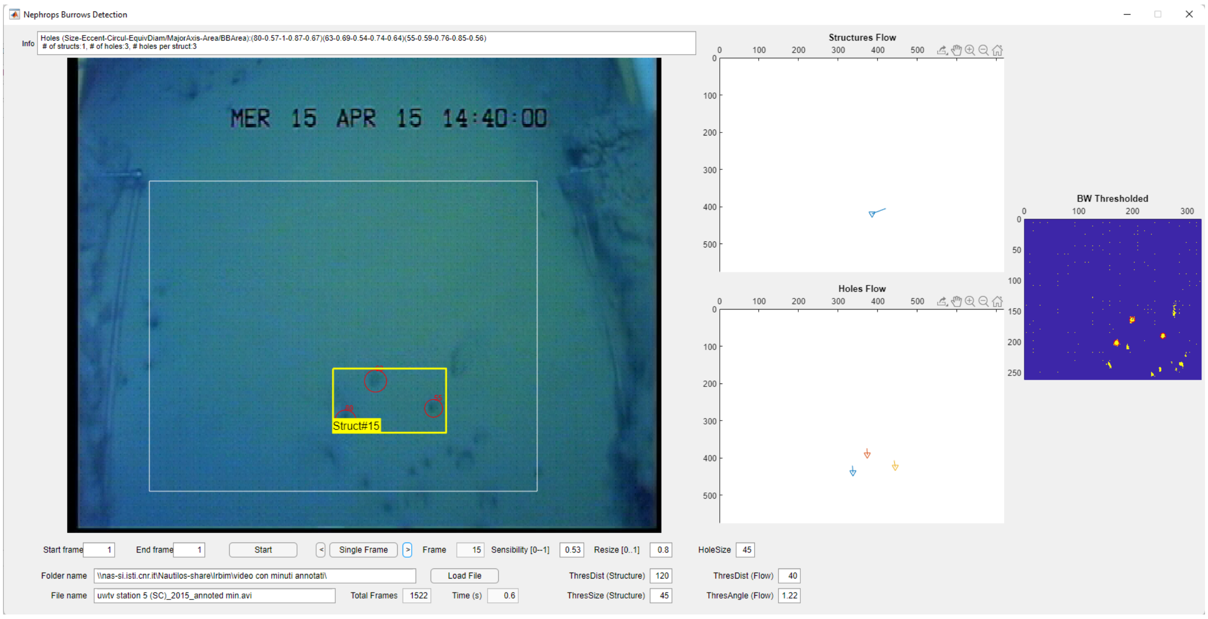

Nephrops Burrows Detection

Info: Holes (Size-Eccent-Circul-EquivDiam/MajorAxis-Area/BBArea):(80-0.57-1-0.87-0.67)(63-0.69-0.54-0.74-0.64)(55-0.59-0.76-0.85-0.56)
# of structs:1, # of holes:3, # holes per struct:3

Start frame 1 | End frame 1 | Start | < | Single Frame | > | Frame 15 | Sensibility [0--1] 0.53 | Resize [0..1] 0.8 | HoleSize 45

Folder name \\nas-si.isti.cnr.it\Nautilos-share\Irbim\video con minuti annotati\ | Load File | ThresDist (Structure) 120 | ThresDist (Flow) 40

File name uwtv station 5 (SC)_2015_annoted min.avi | Total Frames 1522 | Time (s) 0.6 | ThresSize (Structure) 45 | ThresAngle (Flow) 1.22

*Figure 29. Highlight of the holes (lower yellow circle) and structures (upper yellow-circle) optical flows between the current frame and previous one.*

More than one structure can be present on the same frame, and the algorithm is developed to keep track and count them separately. In Figure 30 an example with two different structures was detected, while in Figure 31 an instance with 3 separate structures on the same frame is shown. In both these situations, it can be seen that the tracking of the structures, shown in the upper-right-centre panel, is maintained. For the 2 structures case, the upper one (#8) is not present in the tracking because it is a newly identified structure and thus coloured in red.

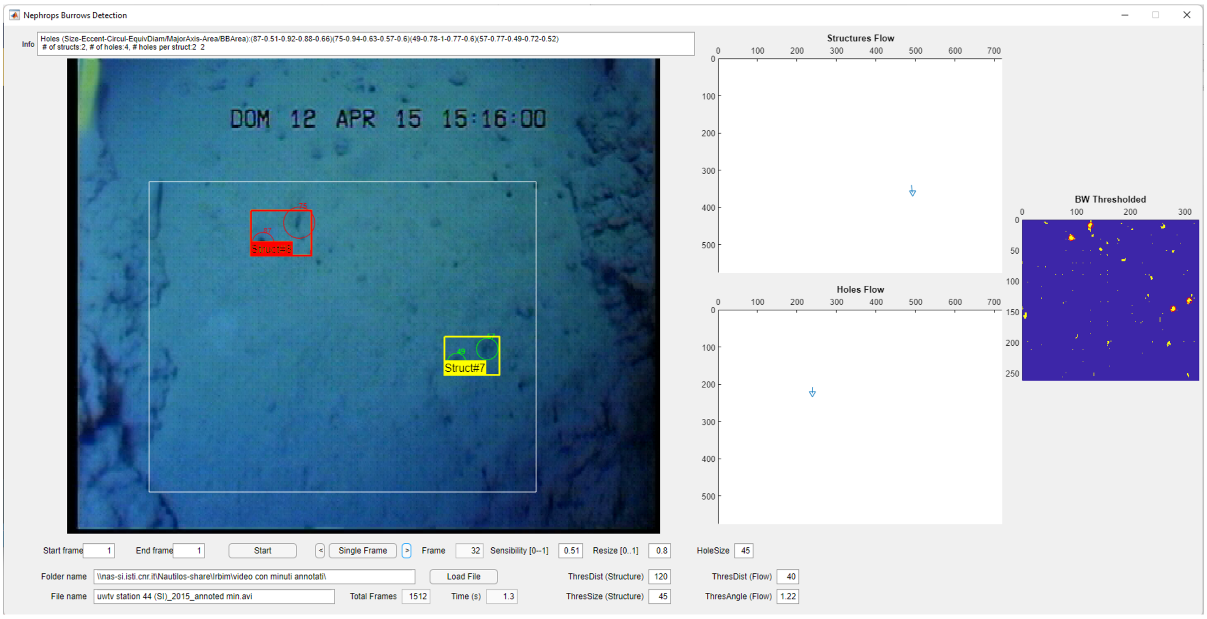
Nephrops Burrows Detection

Info: Holes (Size-Eccent-Circul-EquivDiam/MajorAxis-Area/BBArea):(87-0.51-0.92-0.88-0.66)(75-0.94-0.63-0.57-0.6)(49-0.78-1-0.77-0.6)(57-0.77-0.49-0.72-0.52)
 # of structs:2, # of holes:4, # holes per struct:2  2

Start frame: 1
End frame: 1
Frame: 32
Sensibility [0--1]: 0.51
Resize [0..1]: 0.8
HoleSize: 45
Folder name: \\nas-si.isti.cnr.it\Nautilos-share\Irbim\video con minuti annotati\
ThresDist (Structure): 120
ThresDist (Flow): 40
File name: uwtv station 44 (SI)_2015_annoted min.avi
Total Frames: 1512
Time (s): 1.3
ThresSize (Structure): 45
ThresAngle (Flow): 1.22

Figure 30. Example of multiple structures (2) detected.

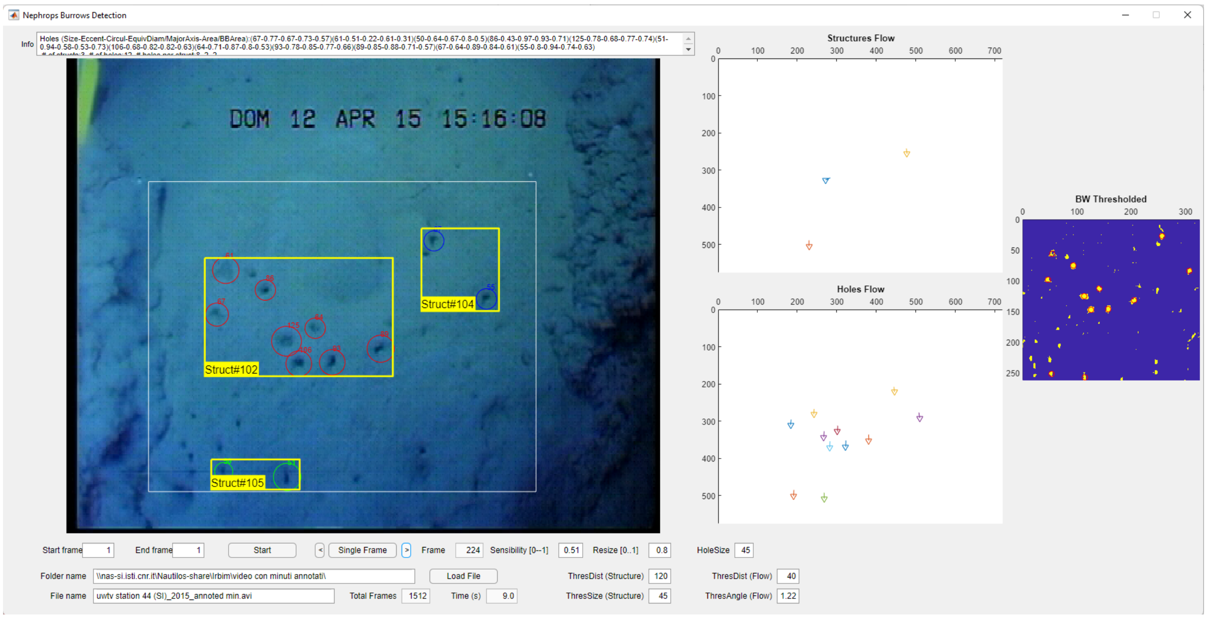
Nephrops Burrows Detection

Info: Holes (Size-Eccent-Circul-EquivDiam/MajorAxis-Area/BBArea):(67-0.77-0.67-0.73-0.57)(61-0.51-0.22-0.61-0.31)(50-0.64-0.67-0.8-0.5)(86-0.43-0.97-0.93-0.71)(125-0.78-0.68-0.77-0.74)(51-0.94-0.58-0.53-0.73)(106-0.68-0.82-0.82-0.63)(64-0.71-0.87-0.8-0.53)(93-0.78-0.85-0.77-0.66)(89-0.85-0.88-0.71-0.57)(67-0.64-0.89-0.84-0.61)(55-0.8-0.94-0.74-0.63)
 # of structs:3, # of holes:12, # holes per struct:8  2  2

Start frame: 1
End frame: 1
Frame: 224
Sensibility [0--1]: 0.51
Resize [0..1]: 0.8
HoleSize: 45
Folder name: \\nas-si.isti.cnr.it\Nautilos-share\Irbim\video con minuti annotati\
ThresDist (Structure): 120
ThresDist (Flow): 40
File name: uwtv station 44 (SI)_2015_annoted min.avi
Total Frames: 1512
Time (s): 9.0
ThresSize (Structure): 45
ThresAngle (Flow): 1.22

Figure 31. Another example with three different structures identified.

In this last example, the structures numbered #102 (with holes in red) and #104 (with holes in blue) are identified as different and separated ones: this is due to differences in the geometry of the two groups of composing holes, as well as due to distances between the composing holes.

On the other hand, the following Figure 32 shows a different example of multiple structures detected where two of them are overlapped. Structure #99 (with red holes) and #101 (with blue holes) are identified as different structures with holes belonging to each separate system due to the various geometric features of the holes themselves and characterising the two systems.

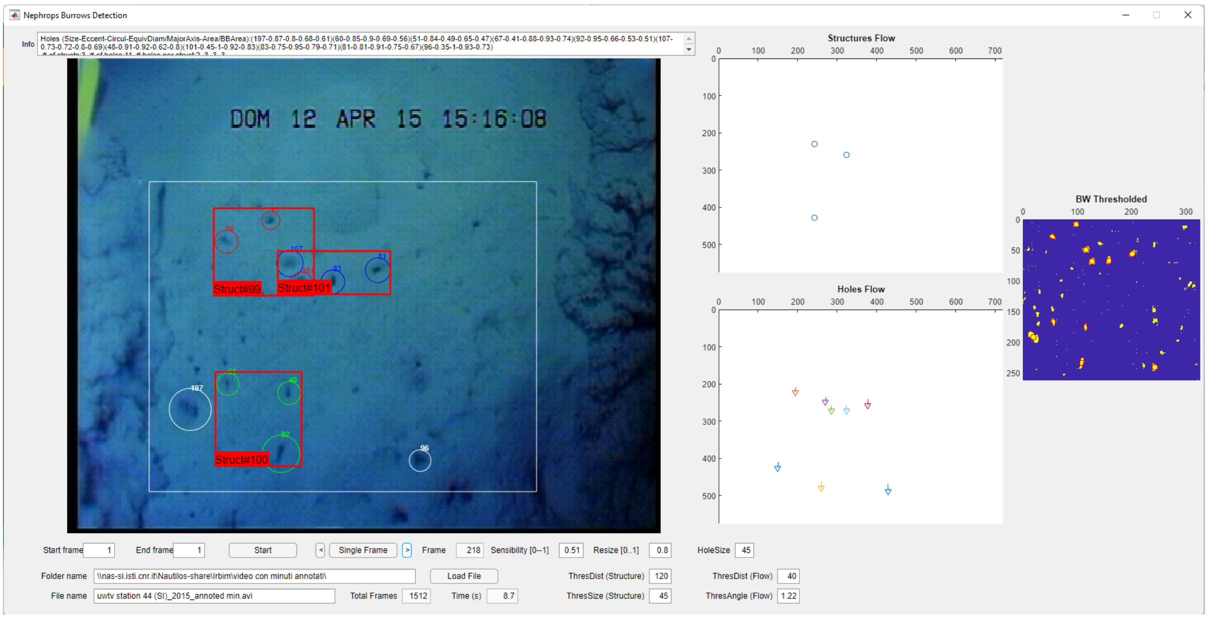
Nephrops Burrows Detection

Info Holes (Size-Eccent-Circul-EquivDiam/MajorAxis-Area/BBArea):(197-0.87-0.8-0.68-0.61)(60-0.85-0.9-0.69-0.56)(51-0.84-0.49-0.65-0.47)(67-0.41-0.88-0.93-0.74)(92-0.95-0.66-0.53-0.51)(107-0.73-0.72-0.8-0.69)(48-0.91-0.92-0.62-0.8)(101-0.45-1-0.92-0.83)(83-0.75-0.95-0.79-0.71)(81-0.81-0.91-0.75-0.67)(96-0.35-1-0.93-0.73)

Start frame 1  End frame 1  Start  <  Single Frame  >  Frame 218  Sensibility [0--1] 0.51  Resize [0..1] 0.8  HoleSize 45

Folder name \\nas-si.isti.cnr.it\Nautilos-share\Irbim\video con minuti annotati\  Load File  ThresDist (Structure) 120  ThresDist (Flow) 40

File name uwtv station 44 (SI)_2015_annoted min.avi  Total Frames 1512  Time (s) 8.7  ThresSize (Structure) 45  ThresAngle (Flow) 1.22

Figure 32. Example of multiple and overlapping structures identified.):

1. a cold water filament going westwards, originating from the southward upwelling jet that runs along the western coast of Portugal;
2. a cold water filament going southwards, extending over Cape St. Vincent the upwelling jet mentioned above;
3. a clear stream of cool water running along the southern Iberian coast;
4. a warm countercurrent originating in the Gulf of Cádiz and running along the southern Iberian coast, eventually reaching Cape St. Vincent and turning northwards.

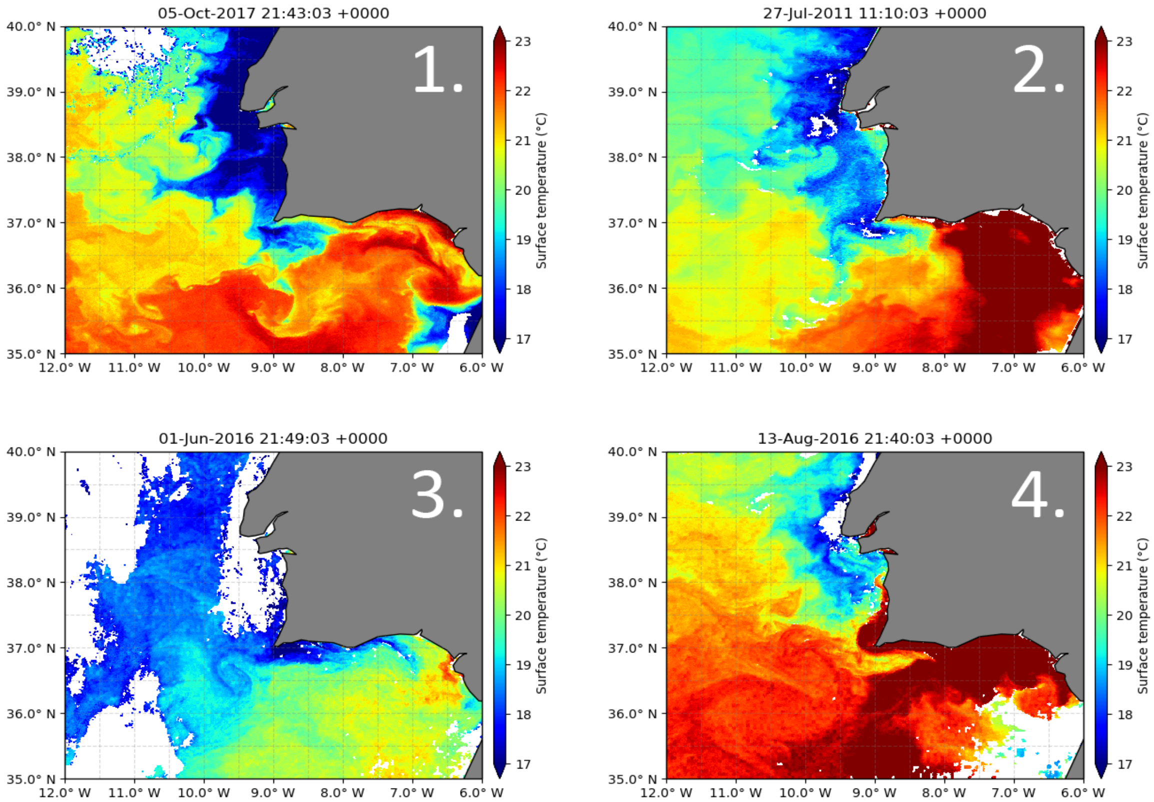

*Figure 1. Examples of patterns identified in SST maps.*

A set of SST maps, where a number between 1 and 4 is assigned by experts to each, form a labelled dataset which can be used as input for some classical supervised automatic classification algorithms. However, several problems arise from this approach due to the peculiar nature of the images:

- depending on the atmospheric conditions at the time of detection (e.g. cloud coverage), the majority of images shows some sort of "noise" which interferes with the outcome of the algorithms;
- even if the satellites provide some hundreds of images per day, only a few of them (usually 2–3 per day) cover, even only partially, the area of interest, and considering that it is likely that some of them are completely useless due to the aforementioned noise, obtaining a large enough labelled dataset requires time and effort;
- the four classes of events appear in nature with uneven frequencies, type 3 being the most common (almost 2 out of 3 recognized patterns belong to it on average), but many classification algorithms need balanced classes—usually this problem can be solved by discarding samples from overnumbered classes, but that is not an option in this case since good-quality images are already so scarce;
- even experts sometimes are unsure about the attribution of an image to a class because of a variety of factors (e.g. two or more events could happen simultaneously and none of them is prominent enough); human errors may also occur during this manual classification;
- usually an upwelling event is present and recognizable for a period of time of 1–2 weeks, but the temporal relation between consecutive images is not taken into account when a label is assigned, except for ambiguous cases.

In Task 8.5 of NAUTILOS, a dedicated tool for the analysis and classification of this dataset has been developed. This tool is described in depth in section IV-**Errore. L'origine riferimento non è stata trovata.**.

## 2. Benthic imagery classification

This section concerns a description of the most relevant approaches in underwater optical image analysis. The description focuses on unsupervised and semisupervised methods for image segmentation purposes.

### 2.1. Segmentation through unsupervised techniques

Underwater imagery capture and analysis is a commonly employed system to perform assessment of marine biodiversity. Amongst the existing approaches the usage of photoquadrat sampling is a largey adopted technique [7]. It consists of collecting images of the seabed holding a rectangular plastic frame, with known dimensions, rigidly fixed in front of the camera. Thus, the frame is constantly kept in the same position within the visual field and, since the plastic frame dimensions are known, this system allows to accurately delimit the surveyed scene and to subsequently perform metric analysis. The analysis usually aims at identifying and grouping the image regions that relate to the various biological specimens, and counting them to estimate the relative samples sizes. The input data undergo preliminary processing stages where the frame is automatically identified through detection of the quadrat area. Calibration and image enhancement can be applied as optional steps. The main biological assessment stage can be implemented by one of the following methods:

a) free hand drawing: it consists in manually assigning labels to the specimen in a quadrat, by directly drawing on the image the contours that enclose each related specimen region. Then, the several user-defined areas can be associated to different biological species and a quantitative assessment on those image subsets is carried out to provide i) the specimen percentage coverage, ii) the areas in metric units, iii) statistics on the population in their habitats, iv) health status of each specimen, etc.

b) grid cell count: this method consists in subdividing the quadrat in a grid of subquadrats and performing the biological assessment described at previous point within each subquadrat.

c) random point count: this method implies the biological assessment through random sampling performed on the set of quadrat image pixels. Given the input image, a number of pixels is randomly chosen and each selected pixel is manually assigned to a category, then the number of individuals for each species is counted and eventually the biological statistics is inferred for each species.

d) automatic image segmentation: this method applies automatic segmentation to the input image based on *statistical region merging* (SRM), proposed in [8]. This method performs a partitioning of the input image in several segments based on a criterion of homogeneity in terms of pixel intensity and color.

The latter method has been claimed to be enough accurate and computationally efficient for the research purposes of the marine biologist. SRM is a region merging algorithm that addresses the image segmentation problem as a statistical test performed between two generic image regions. The formal predicate of the test states that the considered regions can be merged if they are sufficiently similar. The similarity criterion is based on the average values of the pixels' intensities, estimated locally within the considered regions. If the difference between the computed quantities lies below a certain threshold the two regions are considered as part of the same region and they are accordingly merged. The method is completely unsupervised since the mentioned threshold is computed based solely on the pixel cardinalities of the considered regions. The algorithm segments 512x512 images in about 1 second on Intel Pentium® IV 2.40 GHz processor.

### 2.2. Segmentation through semisupervised techniques

Segmentation of underwater imagery can be performed also taking into account the textural information intrinsic in the appearance of the surveyed scenario. Considering the human vision system as a basis for comparison, the surface appearance of objects, as perceived by the eye, is exploited at an early stage to provide a preliminary categorization of the scene. Due to its primary role in human perception it represents a fundamental topic in computer vision, as testified by the plethora of associated literature. Texture is defined as "*a spatial pattern of local surface radiances giving rise to the perception of surface homogeneity*" [9]. Based on this definition many tools have been proposed to capture texture signature and provide the basis for its quantitative assessment. Concerning the image segmentation problem, a popular approach consists in filtering an input image through a bank of Gabor kernels. Their usage has been largely exploited for image segmentation also within the underwater exploration domain [10]. A two-dimensional Gabor kernel is a complex-valued function mapping $\mathbb{R}^2$to $\mathbb{C}$, with the following form:

$$h(x, y) = g(x', y') \cdot \exp[2\pi j(Ux + Vy)]$$

where $(U, V)$ represents the 2D sinusoidal frequency, $(x', y') = (x \cos\phi + y \sin\phi, -x \sin\phi + y \cos\phi)$ are generically rotated coordinates, and $g(x', y')$ is a Gaussian kernel:

$$g(x, y) = \left(\frac{1}{2\pi\lambda\sigma^2}\right) \cdot \exp\left[-\frac{(x/\lambda)^2 + y^2}{2\sigma^2}\right]$$

Hence, $h(x, y)$ is a complex sinusoidal grating modulated by a two-dimensional Gaussian function with aspect ratio $\lambda$, scale parameter $\sigma$, and major axis oriented at an angle $\phi$ from the $x$-axis. Being a sinusoidally modulated Gaussian, the Gabor kernel transforms into another Gaussian shaped function in the Fourier domain, with orientation and frequency properties defined respectively by $\phi$ and $(U, V)$. The convolution of an image with such a kernel entails the selective filtering of those components that share frequency similarities with the modulating sine, and that match with the orientation of the Gaussian kernel. The magnitude of the filtered image will be maximized over those regions of the original image characterized by the particular spatial frequency attributes to which the filter is tuned.

Applying a filter bank to an image, with a properly chosen set of orientation and frequency parameters, returns an array of textural informative values for every pixel. This array can be fed to clustering algorithms, e.g. K-means, to group pixels exhibiting some kind of homogeneity. Eventually, a label is assigned to each cluster, thus fulfilling an unsupervised segmentation task, as proposed in [11].

The described Gabor filters bank has been tested within NAUTILOS to deal with the task of the automatic identification of relevant areas, i.e. potentially representing objects of interest, within underwater imagery of Mediterranean benthos habitats.

## 3. Seafloor fauna detection

This section reports the analysis and state-of-the-art of available image analysis methods dedicated to the detection of specific marine fauna species. Following discussion between NAUTILOS partners, CNR-IRBIM raised the issue of a specific open problem concerning the count of one particular fauna species, the Norway lobster (*Nephrops norvegicus*) [12, 13], a seafloor resident species of mollusc.

Surveys are being conducted to provide fishery-independent stock size estimations of the lobster, based directly on burrow counting using the survey assumption of “one animal = one burrow”. However, stock size may be uncertain depending on true rates of burrow occupation [14]. This problem is studied also in the context of the International Council for the Exploration of the Sea (ICES) with its specific Working Group on Nephrops Surveys (WGNEPS). The main concern is that this counting activities are actually performed manually by several experts manually tagging the recorded underwater videos, and cross-checking the outcomes to have a more precise outcome. As it can be clear such work is very time-demanding, requiring several experts working on the same videos, and it is exposed to the subjectivity of the specific groups of experts. Thus any progress towards an automatic or even semi-automatic processing would be a valuable support in this activity [15].

Focusing on the detection and counting of burrows built by Nephrops individuals, the first analysis reports a wide variety and complexity of the structures (in terms of 3D constructions starting from the opening and down to the bottom) and the appearance of the structures (as they appear from the television recording showing the seafloor) [16]. Furthermore, another difficult issue arises from the differences between diverse areas where this counting needs to be performed, and thus slightly different species or behaviour of this Nephrops. For instance, the samples from the Adriatic sea shows a much higher number of burrows, having a smaller size with respect with Scottish footages, which have much fewer but larger burrows.

As reported by experts and researchers working on this topic, not many studies have been made on this topic, as the existence and reports from ICES-WGNEPS witnesses. Among the few works in literature dealing with this, we identified, as part of the WGNEPS group, the work done in [17] using the deep learning paradigm, which is actually under refinements and shows promising results, although several risks have emerged, such as the need for many manually tagged samples to train the network, as well as the need for different training and testing sets for different reference scenarios (e.g. the various environments and countries where the recordings are made). Moreover, a call for a standardisation effort over these television recordings is made.

No other specific works have been found using other machine vision approaches based on novel promising deep learning paradigms or more consolidated classical criteria. We then decided to develop an approach for supporting automatic detection and counting of burrows, based on a more classical machine vision approach that will be described in detail in section IV-6.

# IV. Developed algorithms

After the environmental domains have been described and the state-of-the-art in each case study, this section presents and discusses in detail the specific algorithms designed and implemented to support domain experts. A particular focus is dedicated to presenting the various user interfaces created for each of the purposes.

## 4. Sea Surface Temperature pattern classification

The manual classification by experts assigns a type of event to a *static* map of the SST in the area at a precise date and time; within the NAUTILOS project, a more *dynamical* approach was followed, where the temporal relations between the SST values registered in a geographical point are organised and analysed. A series of tools for the SST analysis and pattern classification have been developed using the Python 3 programming language.

### 4.1. Plot SST values against time

The first tool extracts the SST information from a set of netCDF files and plots it against time. For simplicity of use, the tool is supplied with a Graphical User Interface (GUI), whose main window is represented in Figure 2. More information on this tool can be found in [18].

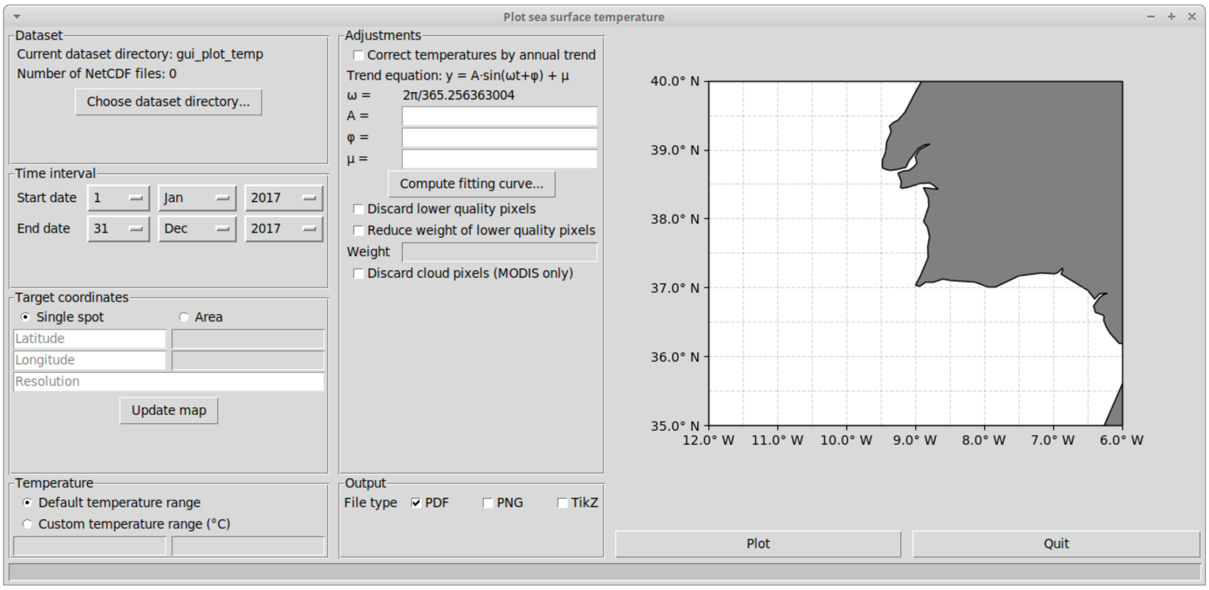

Plot sea surface temperature

Dataset
Current dataset directory: gui_plot_temp
Number of NetCDF files: 0

Time interval
Start date 1 Jan 2017
End date 31 Dec 2017

Target coordinates
● Single spot ○ Area
Latitude
Longitude
Resolution

Temperature
● Default temperature range
○ Custom temperature range (°C)

Adjustments
□ Correct temperatures by annual trend
Trend equation: y = A·sin(ωt+φ) + μ
ω = 2π/365.256363004
A =
φ =
μ =
□ Discard lower quality pixels
□ Reduce weight of lower quality pixels
Weight
□ Discard cloud pixels (MODIS only)

Output
File type ☑ PDF □ PNG □ TikZ

*Figure 2. Main window of the SST plot GUI.*

In the GUI it is possible to select the directory containing the netCDF files and the space and time parameters of the plot. In particular, there are two “modes” for the space coordinates: in “Single spot” mode, the user is asked for a latitude and longitude (expressed in decimal degrees, with positive/negative values representing N/S and E/W respectively) and a resolution (expressed in decimal degrees) such that, if $lat$, $lon$ and $res$ are those values, the SST value for the point with coordinates $(lat, lon)$ for a single netCDF file is computed by averaging all the SST values contained in that file with coordinates in the square $[lat - res/2\,, lat + res/2] \times [lon - res/2\,, lon + res/2]$. This is done because the files are *not* aligned to the grid, meaning that it is not possible to choose an *exact* value for the latitude and longitude that appears in *all* the netCDF files. Typical values for the resolution range between 0.01 and 0.05.

In “Area” mode, the tool produces a plot (*spaghetti plot*) by superimposing all the graphs relative to points in a specified grid. In particular, the four boundaries of the grid (minimum latitude, maximum latitude, minimum longitude, maximum longitude) are specified together with the grid resolution—more precisely, if $lat$, $LAT$, $lon$, $LON$ and $res$ are these values, then each point in the grid has coordinate $(i, j)$ with

$$i \in \{lat, lat + res, lat + 2\,res, \dots, lat + k\,res\},$$
$$j \in \{lon, lon + res, lon + 2\,res, \dots, lon + h\,res\},$$

where $k$ is the minimum value such that $lat + (k+1)\,res \geq LAT$ and $h$ is the minimum value such that $lon + (h+1)\,res \geq LON$. The resulting plot contains a graph for each point with coordinates $(i, j)$ and the SST for that point is computed as the average over the small square $[i, i + res] \times [j, j + res]$. Figure 3 shows an example of a spaghetti plot: graphs relative to neighbouring points are coloured using similar colours, so that it is easier to recognize trends in different zones of the grid.

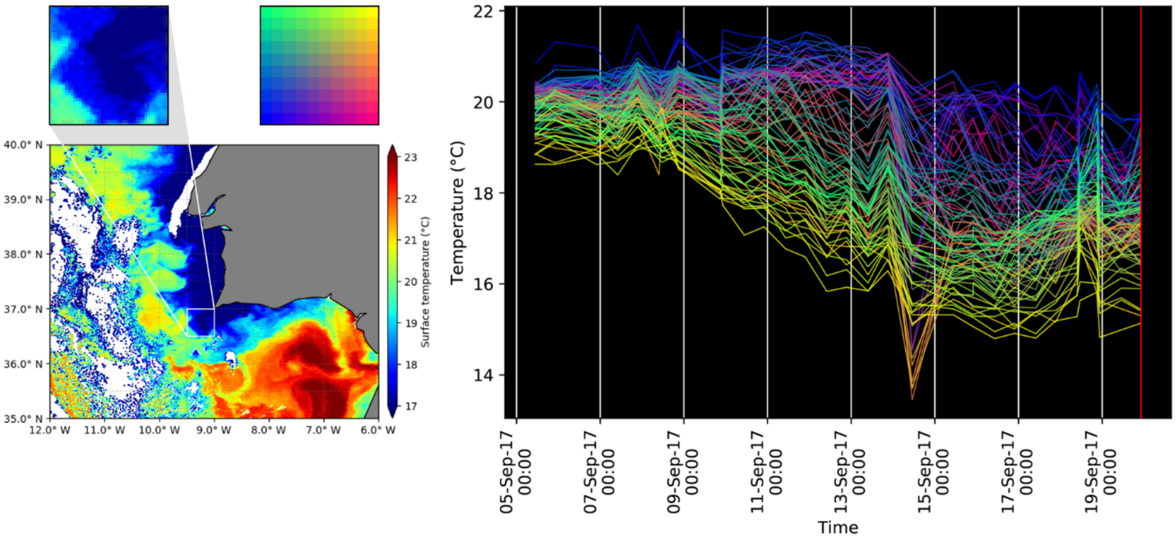

*Figure 3. Example of a spaghetti plot (right). The SST map on the left is relative to a type 3 event identified on 19th September 2017 at 22:13 UTC (corresponding to the red vertical line in the plot on the right). On the top left: detail of the target area for the spaghetti plot (in this case [36.5° N, 37° N]×[9.5° W, 9° W] with a resolution of 0.05°) and reference grid, with each square corresponding to the graph with the same colour in the spaghetti plot.*

A series of adjustments can be performed before producing the plot. First of all, it is possible to take into account the part of the variation in temperature in a period of time due to the natural annual trend, which is assumed to be sinusoidal of the form

$$T(t) = A\ \sin(2\pi t/\omega + \phi) + \mu$$

where $t$ is the time in days, $A$, $\phi$ and $\mu$ are parameters (the tool has a subroutine that is able to compute them by interpolating SST values from a suitable dataset; they can also be provided directly, in case they have been computed previously) and $\omega = 365.256363004$ is the duration of the sidereal year. Figure 4 shows an example of interpolation for the year 2017. In particular, if $SST(t)$ is the SST value at time $t$, with this adjustment enabled the tool produces plots of the function $SST'(t) = SST(t) - (T(t) - T(t_0))$ instead, where $t_0$ is the starting time of the plot; it is assumed that the SST is exact at time $t_0$. The difference between the plots with and without correction is small, as is shown in Figure 5.

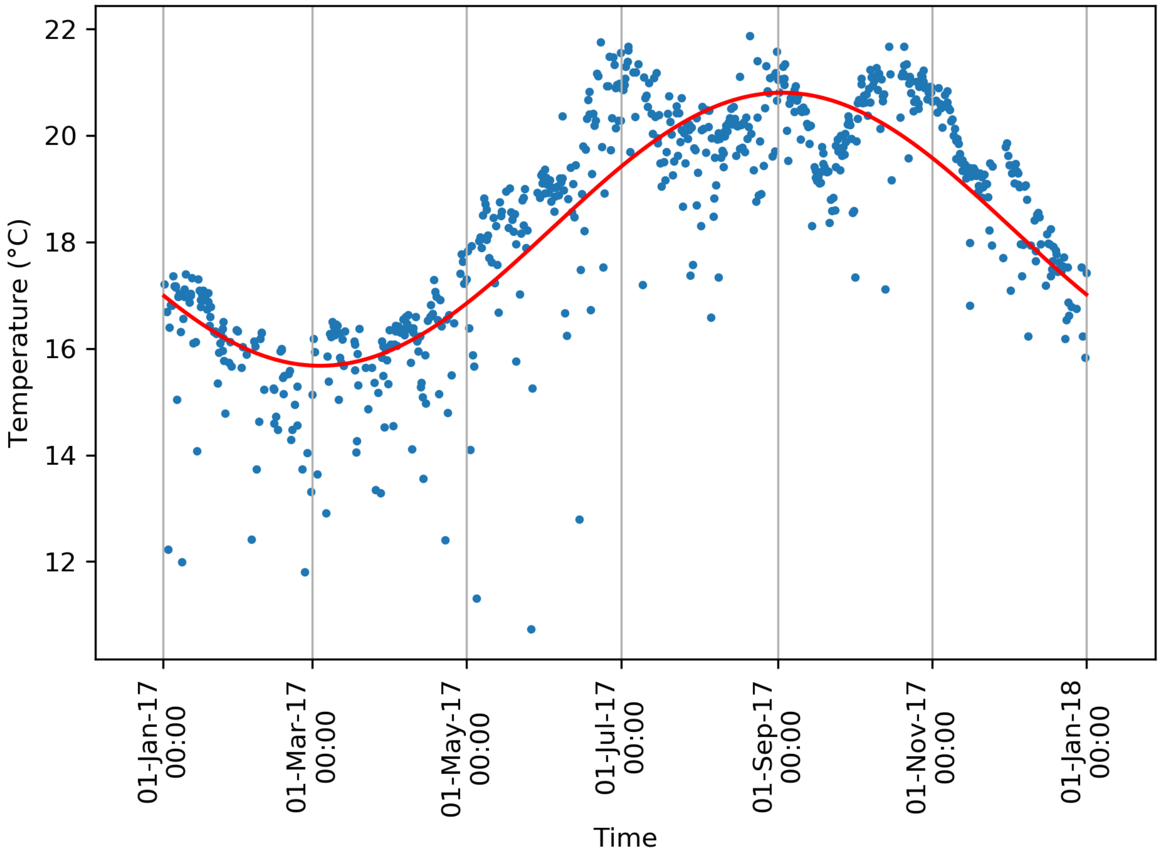

*Figure 4. SST annual trend for 2017 in the window [36° N, 37° N]×[10° W, 9° W]. The blue dots represent the average SST in the window; the red line is the interpolated curve. In this case $A = -2.564578038371188$, $\phi = 0.9652411407664284$, $\mu = 18.242557839045013$.*

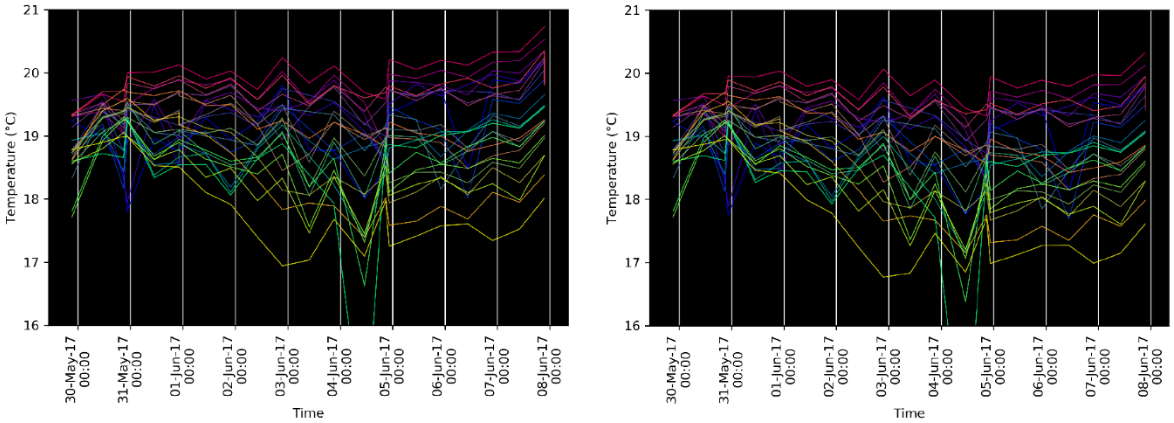

*Figure 5. Spaghetti plots relative to the same area as Figure 4 and the same period of time. On the left: no adjustment is applied; on the right: values are modified according to the assumed annual SST trend.*

Another possible adjustment regards if and how "bad quality" data is considered. Recall that the netCDF files have a layer that describes the quality of the data inside them. The tool is able to either discard completely SST values that are marked as "bad quality" inside the files, or give them a lower weight when computing the averages, with the value of this weight given by the user.

The last adjustment is possible only for the Aqua dataset: among metadata in those files there is the "cloud" mask; the tool is able to discard a SST value if the point is marked as cloud-covered in the netCDF file.

A preliminary analysis of some spaghetti plots produced with this tool already shows some promising results in recognizing patterns of SST trends [19, 20].

### 4.2. Custom Python classes for SST data management

Since the extraction of data directly from the netCDF files may take a long time, depending on the extension of the time period and on the resolution chosen, two custom Python classes have been defined for the storage and management of the SST data: *SpaghettiData* and *SpaghettiPlot*. Detailed technical information about these two classes can be found in [21]; here the main features are reported.

An object of the SpaghettiData class stores information about the SST values in a single geographical point for a period of time; more precisely, given a latitude $lat$, a longitude $lon$ and a resolution $res$, it contains a list of pairs $(t, SST(t))$ where $t$ is a date/time reference and $SST(t)$ is the SST value computed as average on the square $[lat, lat + res] \times [lon, lon + res]$.

Despite all the adjustments described in the previous section, it is possible that bad quality data from some netCDF files may be used to populate a SpaghettiData object (e.g. the satellite may register some low temperature, which at human eye appears clearly incoherent with the temperatures in that point in the days around, but it fails to label it as "bad quality" data). To try to remove this outlier values, a "regularizing" tool has been developed. It can operate in two modes:

- in "discard" mode, first of all the standard deviation $\sigma$ of the series of SST values in the SpaghettiData object is computed; then, for each pair $(t_i, SST(t_i))$ the two previous ($t_{i-2}$, $t_{i-1}$) and the two next ($t_{i+1}$, $t_{i+2}$) timestamps in the SpaghettiData object are considered and the median $m$ of the set $\{SST(t_{i-2}), SST(t_{i-1}), SST(t_i), SST(t_{i+1}), SST(t_{i+2})\}$ is computed; the pair $(t_i, SST(t_i))$ is removed from the object if $SST(t_i)$ does not belong to the interval $[m - x\sigma, m + x\sigma]$ where $x$ is a fixed value (for example $x = 1.5$);
- in "replace" mode, for each pair $(t_i, SST(t_i))$ the previous $(t_{i-1})$ and the next $(t_{i+1})$ timestamps in the SpaghettiData object are considered and the median $m$ of the set $\{SST(t_{i-1}), SST(t_i), SST(t_{i+1})\}$ is computed; the pair $(t_i, SST(t_i))$ is then replaced in the SpaghettiData object with the pair $(t_i, m)$.

Figure 6 shows an example of the effects of the regularization.

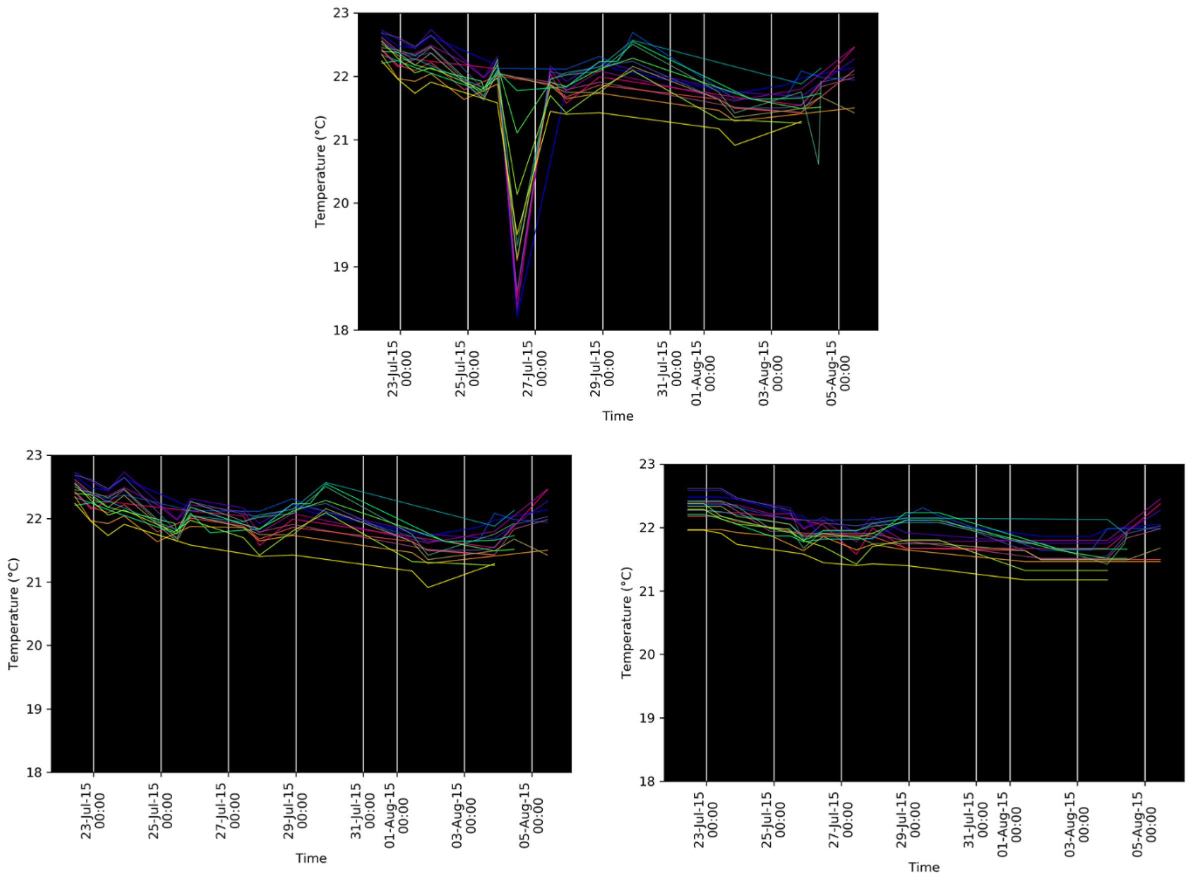

*Figure 6. Top: example of spaghetti plot before the regularization; bottom: the same spaghetti plot after regularization, on the left with mode "discard" and on the right with mode "replace".*

An object of the SpaghettiPlot class is essentially a coherent collection of SpaghettiData objects, with additional features that help to produce plots easier. Given a rectangular area in terms of minimal and maximal latitudes and longitudes, and a resolution, this area is divided into a grid in the same way as the “Area” mode of the tool described in section 4.1; the SpaghettiPlot object contains one SpaghettiData object for each point $(i, j)$ of the grid, such that the reference latitude and longitude for the SpaghettiData object are $i$ and $j$ respectively, and its resolution matches the one of the SpaghettiPlot object.

### 4.3. Mobile windows

If it is possible to plot the SST by extracting the information directly from the netCDF files, thanks to the GUI described in section 4.1, the data structures defined through the Python classes described above allow a more systematic approach. In fact, theoretically one could produce a “big” spaghetti plot covering *all* the area of interest (recall that in this case of study it is the rectangle [35° N, 40° N]×[12° W, 6° W]); however, the huge amount of superimposed graphs, in particular if the resolution is small, would make this plot unreadable.

One possible solution is to produce a collection of SpaghettiData objects containing SST information for all the points of the area of interest for a particular period of time, and then generate spaghetti plots relative to a smaller target window with fixed dimension (e.g. a square of 0.5°×0.5° in latitude/longitude) that shifts, covering the entire area (i.e. a *mobile window*).

A specific tool for producing all these spaghetti plot has been developed. It takes as input the collection of SpaghettiData objects, the limits of the area of interest, the dimensions of the mobile window and the stride, and produces all the spaghetti plots relative to the positions of the mobile window (Figure 7 shows some examples). The aim is to identify patterns in SST trends by studying spaghetti plots relative to areas where experts identified upwelling events.

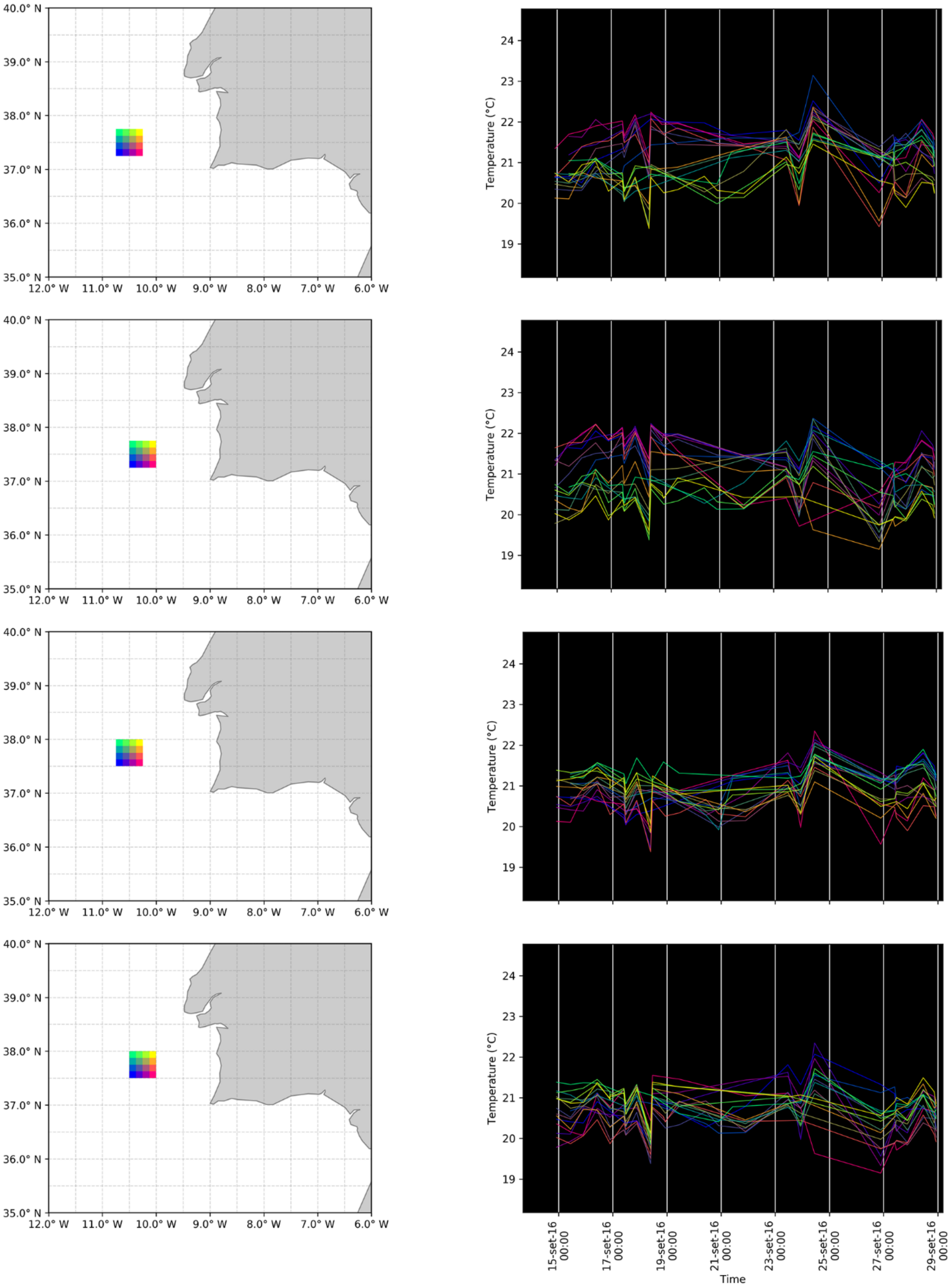

*Figure 7. Example of spaghetti plots produced with the mobile window tool. In this case a 0.5°×0.5° window has been selected, with a resolution of 0.125° and a stride of 0.25°.*

### 4.4. Statistics analysis and classification

All the spaghetti plots relative to areas in which experts have identified SST patterns linked to upwelling events have been analysed in search for patterns in the SST trends. The objective is to attribute numerical values to each SpaghettiData object, so that a set of classification rules could be defined depending on those values. The chosen *statistics* for a single SpaghettiData object are:

- the *mean* of all the SST values;
- the *standard deviation* of all the SST values;
- the *regression coefficient*, i.e. the slope of the regression line computed from the pairs $(t, SST(t))$.

Moreover, the *number of SST values* contained in a SpaghettiData object is chosen as an index of reliability, meaning that statistics computed from too few data are more likely to produce unreliable results.

In order to help analysing the statistics, a tool for their visualisation has been developed (see Figure 8).

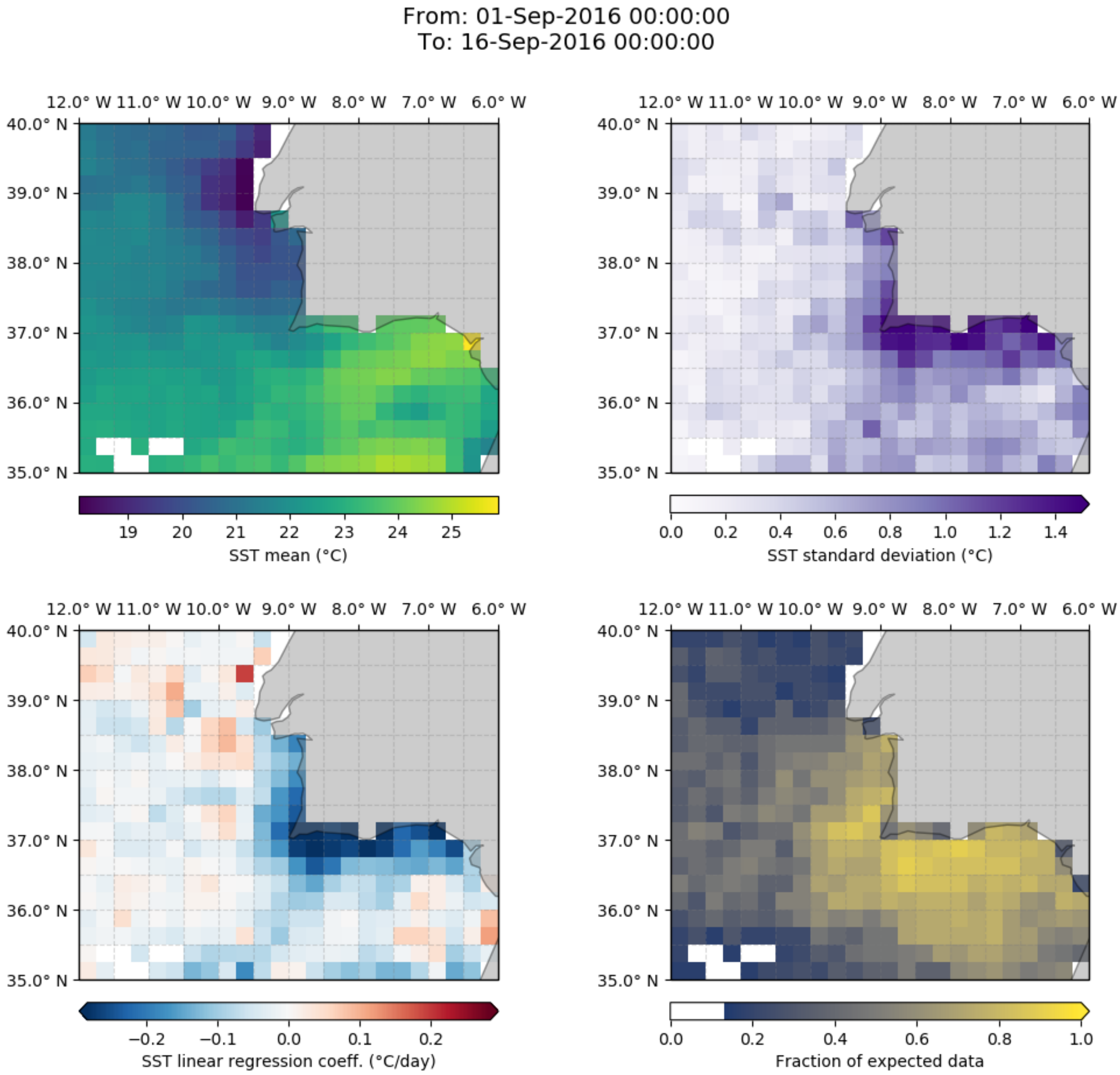

*Figure 8. Visual representation of the statistics for SpaghettiData objects in the area of interest, in the period of 15 days from 1st to 15th September 2016, with SpaghettiData objects with resolution 0.25°. The expected number of data is two SST values per day (i.e. 30 values in a 15-day period), and SpaghettiData objects with less than 5 values are discarded.*

For the classification task, a set of rules has been drafted. The rules assign four scores, one for each of the types of event (hereby called E1, E2, E3 and E4), to each point in the map, according to the values of the statistics both in that point and in neighbouring ones. The rules chosen are summarized in the following list; for a square $(i,j)$, the mean, the standard deviation and the regression coefficient are denoted by $\mu(i,j)$, $\sigma(i,j)$ and $r(i,j)$ respectively; moreover, the neighbouring points of $(i,j)$ are denoted with abbreviations depending on their relative position with respect to $(i,j)$:

| | | | | |
|---|---|---|---|---|
| | | $NN$ | | |
| | $NW$ | $N$ | $NE$ | |
| $WW$ | $W$ | $(i,j)$ | $E$ | $EE$ |
| | $SW$ | $S$ | $SE$ | |
| | | $SS$ | | |

For E3 and E4 rules, an additional notation is necessary: the *coastal neighbourhood* of a point $(i, j)$ is the set

$$N(i, j) = \{x \in \{N, S, W, E, NN, SS, WW, EE, NW, SE\} \text{ such that } |c(x) - c(i, j)| \leq 1\}$$

where $c(i, j)$ is a function that measures the distance of the point $(i, j)$ from the coastline as the minimum of the values $\sqrt{(i-l)^2 + (j-m)^2}$ where $(l, m)$ varies in the set of all coastal points; in addition to this, the *northwestern* and *southeastern neighbourhoods* of $(i, j)$ are the sets

$$N_{NW}(i, j) = N(i, j) \cap \{N, W, NN, WW, NW\},$$
$$N_{SE}(i, j) = N(i, j) \cap \{S, E, SS, EE, SE\}.$$

1. Rules for E1. A point $(i, j)$ gets a score for E1 only if its temperature decreases at a certain rate, i.e. $r(i, j) < -0.05$ and $\sigma(i, j) > 0.2$. In this case:
   1.1. if the point $E$ also decreases in temperature, and does before $(i, j)$, i.e. $r(i, j) > r(E)$: +6 points;
   1.2. if the point $EE$ also decreases in temperature, and does before $(i, j)$, i.e. $r(i, j) > r(EE)$: +3 points;
   1.3. if both the two previous rules are applied, and also the regression coefficients are sorted as $r(i, j) > r(E) > r(EE)$: +2 points;
   1.4. if on average $(i, j)$ is colder than the points to its north, i.e. $\mu(i, j) < \text{mean of } \{\mu(NW), \mu(N), \mu(NE)\}$: +4 points;
   1.5. if on average $(i, j)$ is colder than the points to its south, i.e. $\mu(i, j) < \text{mean of } \{\mu(SW), \mu(S), \mu(SE)\}$: +4 points;
   1.6. if both the two previous rules are applied: +2 points.
2. Rules for E2. A point $(i, j)$ gets a score for E2 only if its temperature decreases at a certain rate, i.e. $r(i, j) < -0.05$ and $\sigma(i, j) > 0.2$. In this case:
   2.1. if the point $N$ also decreases in temperature, and does before $(i, j)$, i.e. $r(i, j) > r(N)$: +6 points;
   2.2. if the point $NN$ also decreases in temperature, and does before $(i, j)$, i.e. $r(i, j) > r(NN)$: +3 points;
   2.3. if both the two previous rules are applied, and also the regression coefficients are sorted as $r(i, j) > r(N) > r(NN)$: +2 points;
   2.4. if on average $(i, j)$ is colder than the points to its east, i.e. $\mu(i, j) < \text{mean of } \{\mu(NE), \mu(E), \mu(SE)\}$: +4 points;
   2.5. if on average $(i, j)$ is colder than the points to its west, i.e. $\mu(i, j) < \text{mean of } \{\mu(NW), \mu(W), \mu(SW)\}$: +4 points;
   2.6. if both the two previous rules are applied: +2 points.
3. Rules for E3. A point $(i, j)$ gets a score for E3 only if its temperature decreases at a certain rate, i.e. $r(i, j) < -0.05$ and $\sigma(i, j) > 0.2$. In this case:
   3.1. if all the other points of $N(i, j)$ also decrease in temperature, i.e. $r(x) < 0$ for all $x \in N(i, j)$: +5 points;
   3.2. if the points to the northwest of $(i, j)$ decrease in temperature before $(i, j)$: +2$n$ points, where $n$ is the number of points $x \in N_{NW}(i, j)$ such that $r(i, j) > r(x)$;

   3.3. if the points to the southeast of $(i, j)$ decrease in temperature after $(i, j)$: +$k$ points for each $x \in N_{SE}(i, j)$ such that $r(x) > r(i, j)$, where $k = 3$ for $x = S$ or $E$ and $k = 2$ otherwise;
   3.4. if on average $(i, j)$ is warmer than the points to its northwest, i.e. $\mu(i, j) > \text{mean of } \{\mu(x) \text{ for } x \in N_{NW}(i, j)\}$: +4 points;
   3.5. if on average $(i, j)$ is colder than the points to its southeast, i.e. $\mu(i, j) < \text{mean of } \{\mu(x) \text{ for } x \in N_{SE}(i, j)\}$: +4 points;
   3.6. if both the two previous rules are applied: +2 points.
4. Rules for E4. A point $(i, j)$ gets a score for E4 only if its temperature increases at a certain rate, i.e. $r(i, j) > 0.05$ and $\sigma(i, j) > 0.2$. In this case:
   4.1. if all the other points of $N(i, j)$ also increase in temperature, i.e. $r(x) > 0$ for all $x \in N(i, j)$: +5 points;
   4.2. if the points to the southeast of $(i, j)$ increase in temperature before $(i, j)$: +$2n$ points, where $n$ is the number of points $x \in N_{SE}(i, j)$ such that $r(i, j) > r(x)$;
   4.3. if the points to the northwest of $(i, j)$ increase in temperature after $(i, j)$: +$k$ points for each $x \in N_{NW}(i, j)$ such that $r(x) > r(i, j)$, where $k = 3$ for $x = N$ or $W$ and $k = 2$ otherwise;
   4.4. if on average $(i, j)$ is warmer than the points to its northwest, i.e. $\mu(i, j) > \text{mean of } \{\mu(x) \text{ for } x \in N_{NW}(i, j)\}$: +4 points;
   4.5. if on average $(i, j)$ is colder than the points to its southeast, i.e. $\mu(i, j) < \text{mean of } \{\mu(x) \text{ for } x \in N_{SE}(i, j)\}$: +4 points;
   4.6. if both the two previous rules are applied: +2 points.
5. Global rules.
   5.1. (*high variation*) if the SST variation is significant, that is $\sigma(i, j) > 1$ and either $r(i, j) < -0.1$ (for E1, E2 and E3) or $r(i, j) > 0.1$ (for E4): +1 point;
   5.2. (*global temperature*) if on average $(i, j)$ is either "cold" (for E1, E2 and E3) or "warm" (for E4), meaning that $\mu(i, j)$ is less (resp. greater) than the mean of all the values $\mu(x)$ for all the points $x$ in the area of interest: the score gets a boost of ×1.2;
   5.3. (*coast distance*) according to the experts, E1- and E2-type events happen far from the coast, whereas E3- and E4-type events happen near the coast; so if either $c(i, j) \leq 3$ (for E1 and E2) or $c(i, j) > 3$ (for E3 and E4): the score gets a penalty of ×0.5.

The scores for each point are then normalized in the interval [0,1] according to the maximum score that can be achieved (see Figure 9).

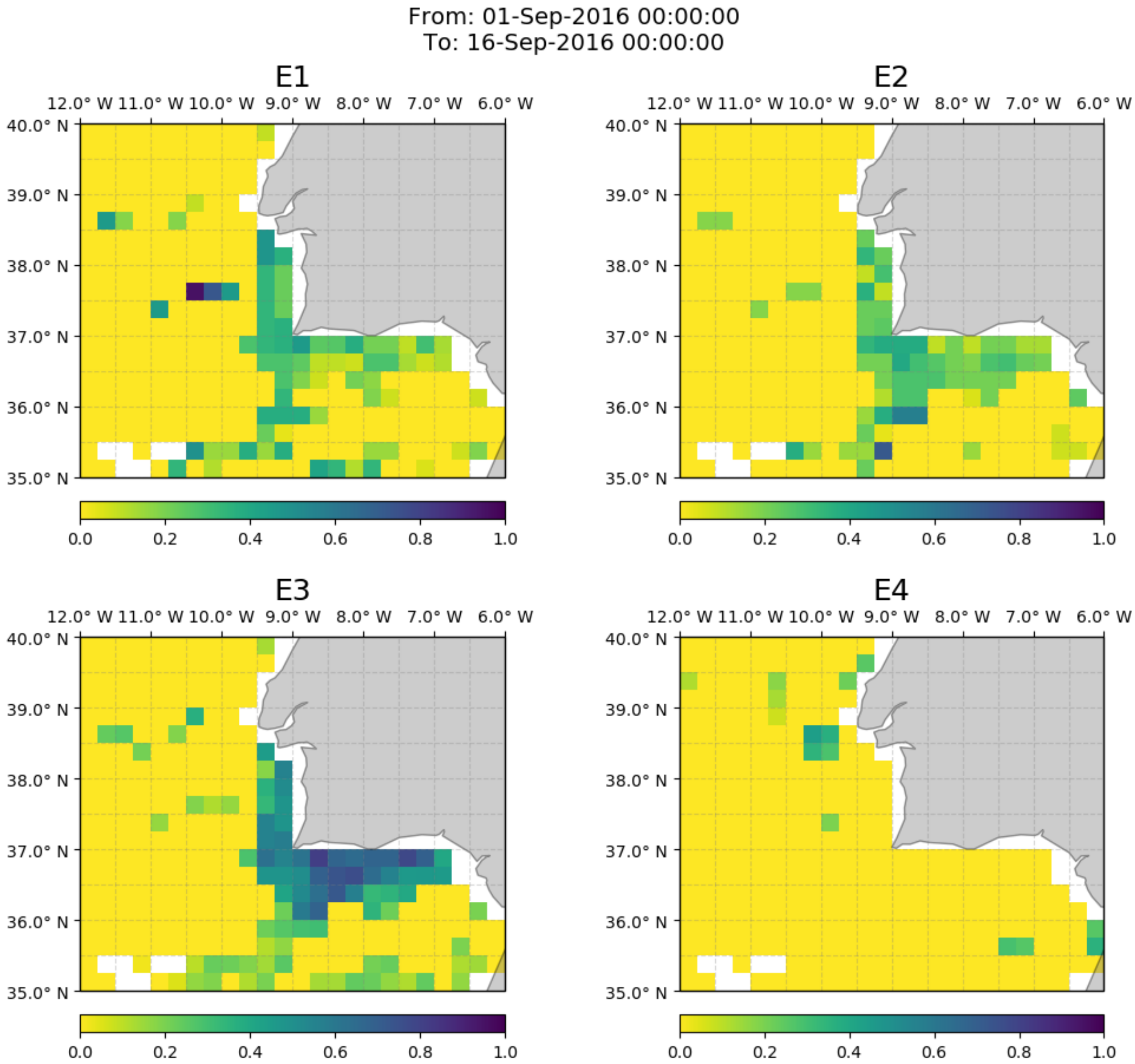

*Figure 9. Scores for the squares computed according to the values of the statistics in Figure 8.*

In order to get a unique label among “E1”, “E2”, “E3”, “E4” or “nothing” for each point $(i, j)$, all the scores are compared and the results are organised in a single “heatmap”, where each point $(i, j)$ is coloured according to the maximal (normalized) scores, but only if this score is greater than a certain threshold (set to 0.6). This map reports also the fraction (as a percentage) of expected data for each classified square, so that it is easy to have an idea of the reliability of the classification at a glance (see Figure 10).

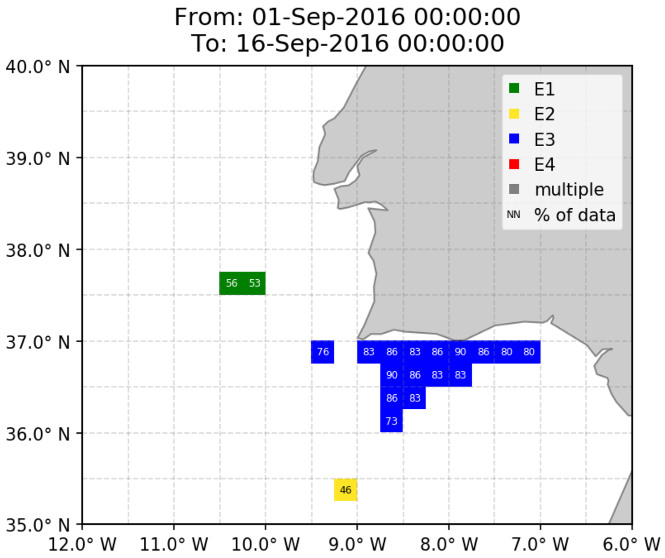

*Figure 10. Heatmap obtained from the scores of Figure 9. The tool finds a prevalent E3 event along the coast and traces of E1 and E2 events.*

This instrument is provided to experts as a decision support tool, helping them to analyse large sets of images by identifying areas that are more likely to show upwelling events; their trained eye can confirm or disprove its results, and their opinions in the latter case can be used to refine the set of rules described above in order to improve the accuracy and reliability.

## 5. Benthic imagery classification

This section describes the preliminary implementation of a software module dedicated to the segmentation of underwater images. The specific typology of data captured for the mentioned purpose consists of high resolution imagery captured by optical sensors. Examples are presented in Figure 11.

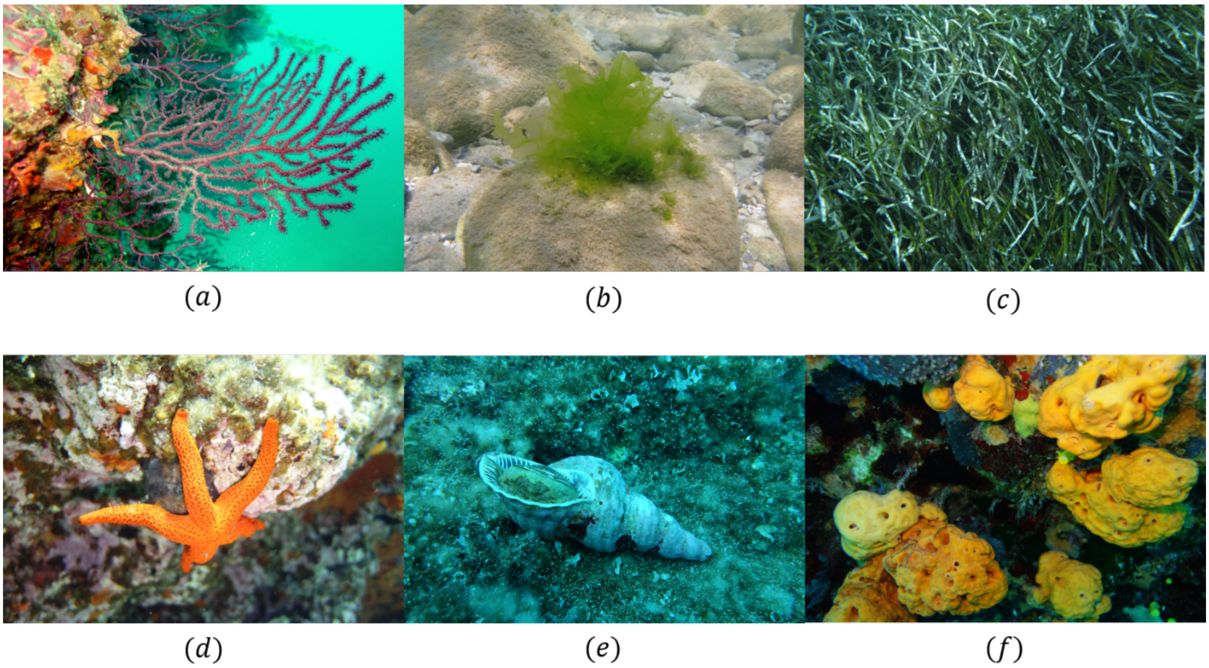
$(a)$ $(b)$ $(c)$

$(d)$ $(e)$ $(f)$

*Figure 11. HCMR Dataset examples: (a) coral; (b) macroalga; (c) seagrass; (d) seastar; (e) mollusc; (f) sponge.*

These images have been provided for testing purposes by the Hellenic Centre for Marine Research (HCMR), which is partner of the NAUTILOS consortium. They represent a documentation of sessile species in the Mediterranean benthic habitat, entirely located within the Greek archipelagus. The dataset consists of 165 color images, with dimensions ranging from 4000x3000 to 5472x3648 pixels, captured by expert divers through handheld cameras. The dataset has been arranged in six categories (corals, macroalgae, molluscs, seagrass, seastars and sponges), each in turn subdivided in several subcategories. Every image displays one single individual species out of those documented, typically represented as the foreground object. This dataset accounts for the biodiversity associated to the specific geographical location.

In this framework, the goal of the underwater biologist is to perform an assessment about the species detected in the surveyed scene, estimate the amount of individuals for each typology, evaluate the population health status and provide related statistics. A software module supporting this task has been studied and designed, with the goal of performing automatic segmentation of the observed biological specimen, to be later exploited for a biological species classification stage. Some preliminary attempts have been performed, implementing software tests in a MATLAB (from MathWorks® version R2019b) environment. The main approach adopted here consists of performing image segmentation to discriminate between foreground and background. Basically, the procedure consists in grouping the captured image pixels following a homogeneity criterion directly applied to the pixels' intensities, or to the output of an intermediate processing level aimed at extracting informative features.

### 5.1. Clustering pixel intensities

The dataset imagery nature is largely variable in terms of a number of parameters, among which we can mention the environmental illumination, the biological species type, the foreground morphology, its color properties and the unavoidable presence of multiple benthic specimen within the same observed scenario. All that contributes to enlarge the task complexity and makes it unfeasible to propose a segmentation procedure based on a univocal criterion.

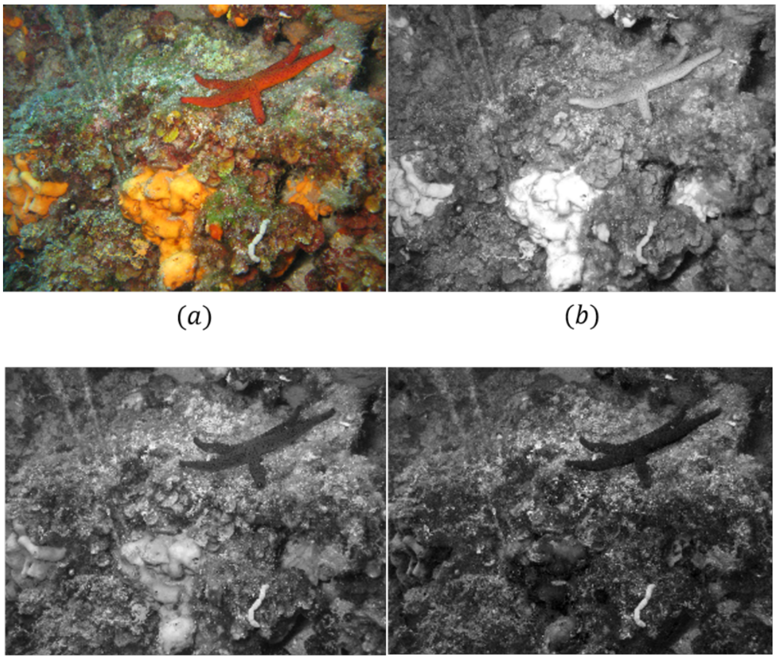

*Figure 12. Input image example (a) and the related RGB channels (b)-(d).*

As a first attempt the data has been directly processed through grouping algorithms (K-means) based on the exploitation of the pixels' intensities.

Looking at the dataset it is undeniable that color information plays a primary role in the description of underwater biodiversity. Thus, the input images undergoes a first transformation from RGB (Figure 12) space to CIE Lab space (Figure 13). In this space the visual differences ascribed to color can be easily quantified, regardless of brightness variations. Indeed, the difference between two colors can be measured using a Euclidean distance metric applied to the chromaticity layers a* and b*.

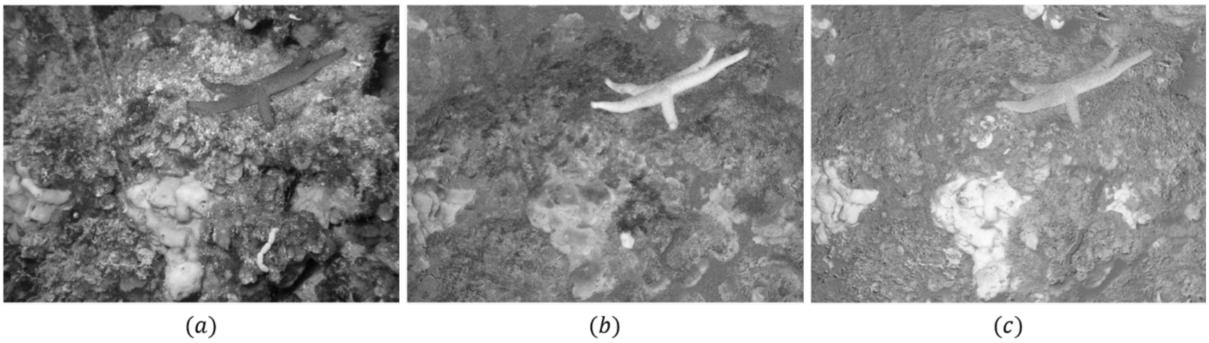

*Figure 13. CIE Lab representation: (a) brightness channel L; (b) chromaticity channel a*; (c) chromaticity channel b*.*

The converted image is then processed by the K-means algorithm to group pixels belonging to the same category. K-means finds partitions of the image such that pixels belonging to the same category are as close to each other as possible, and as far from objects in other clusters as possible.

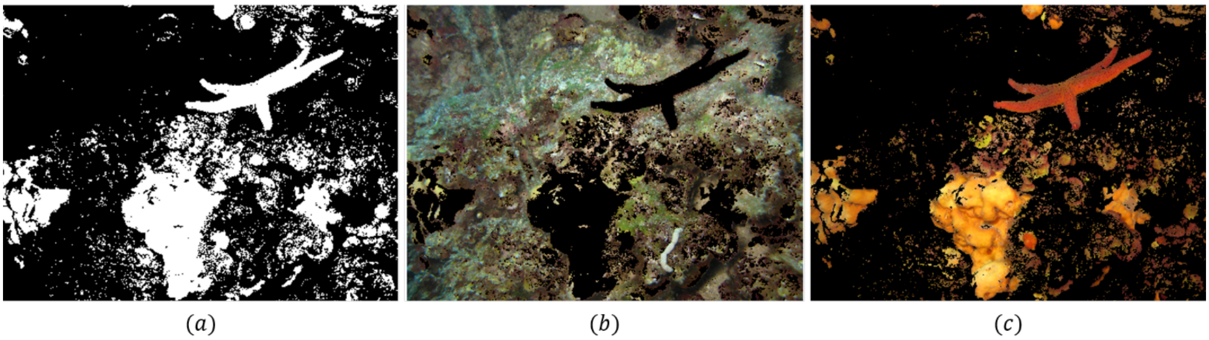

*Figure 14. K-means clustering with two classes applied to an HCMR image. (a) binarized image with cluster labels; (b) cluster I; (c) cluster II.*

The K-means algorithm is semi-supervised, meaning that it automatically assigns a cluster label to each pixel, but the number of classes needs to be known in advance. Figure 14 represents the output resulting from applying K-means to cluster pixels in an image, extracted from the HCMR dataset, into two clusters, while the same operation specifying three classes in input, is shown in Figure 15.

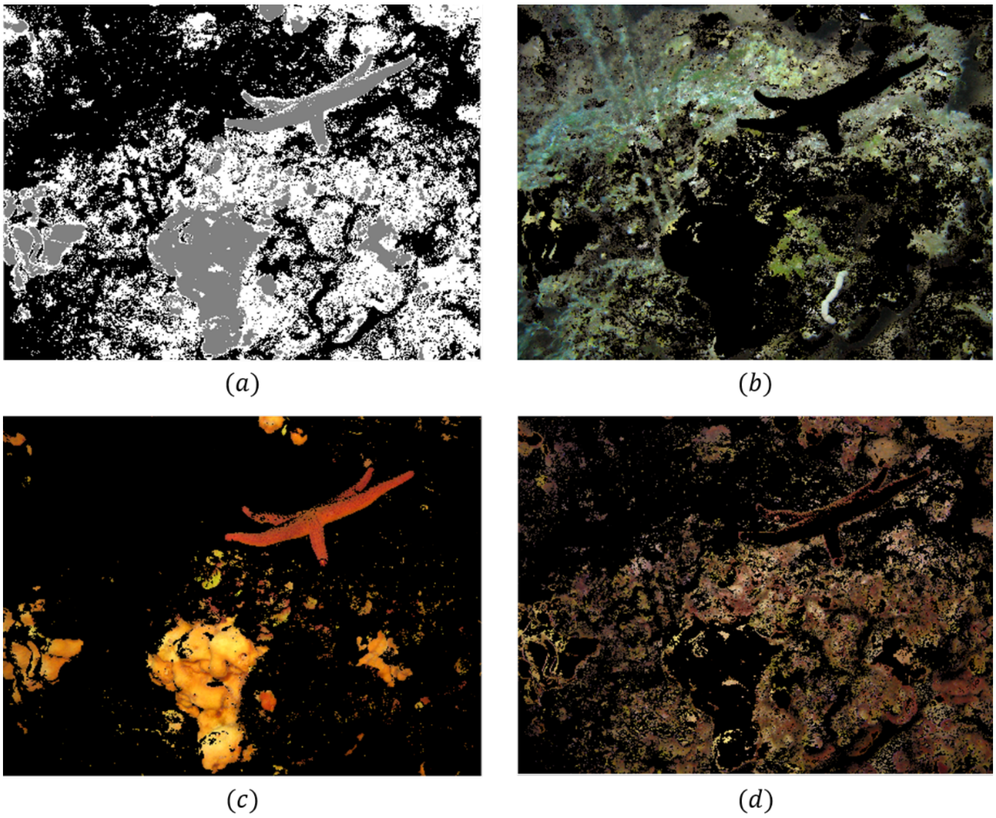

*Figure 15. K-means clustering with three classes applied to an HCMR image. (a) binarized image with cluster labels; (b) cluster I; (c) cluster II; (d) cluster III.*

It is apparent that accurately separating different species represented in the same image is a non trivial goal, hard to obtain even increasing the number of classes. This may be due to the poor discriminative power of the pixels' intensity feature, which may not be a sufficiently informative feature to separate the clusters, especially in the case that two distinct objects exhibit similar color properties.

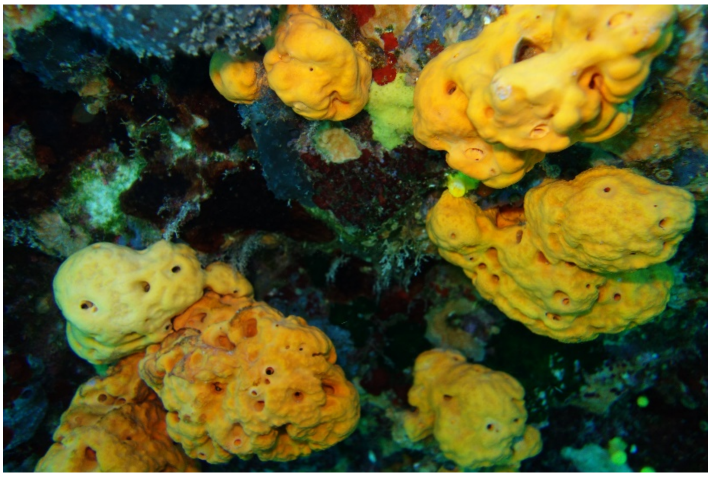

*Figure 16. Orange sponge specimen (HCMR dataset).*

Another example of the application of this procedure is reported in Figure 16, where a single sponge specimen is observed.

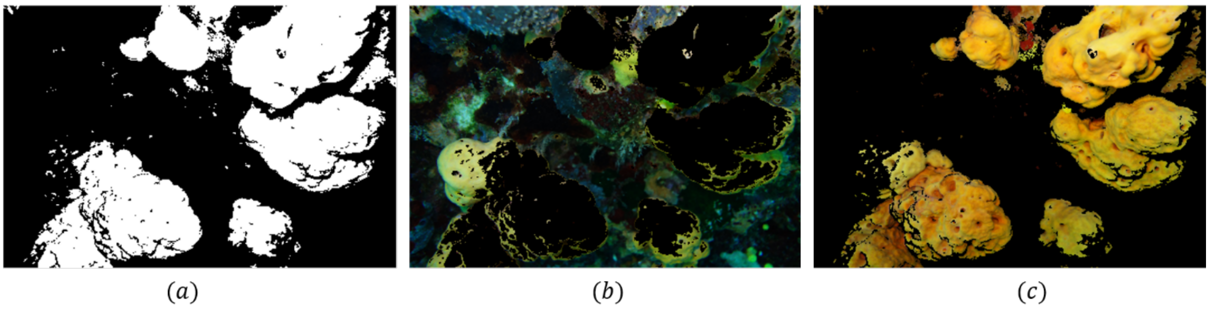

*Figure 17. K-means clustering with two classes applied to an HCMR image of a sponge. (a) binarized image with cluster labels; (b) cluster I; (c) cluster II.*

In this case the observed specimen occupies a large image area and is clearly observed as a foreground object. The application of K-means with two (Figure 17) or three classes (Figure 18) as input parameters returns similar results in terms of foreground/background separation.

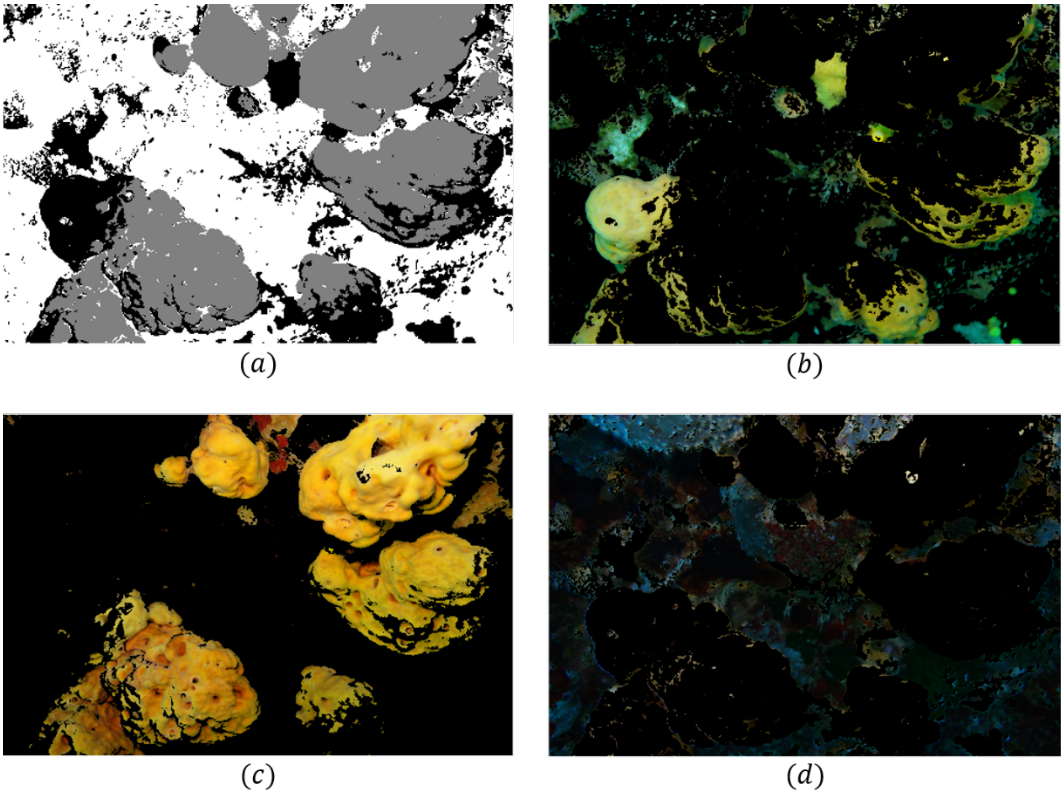

*Figure 18. K-means clustering with three classes applied to an HCMR image of a sponge. (a) binarized image with cluster labels; (b) cluster I; (c) cluster II; (d) cluster III.*

### 5.2. Clustering image features

Grouping pixels solely based on the color properties is not sufficient for the segmentation task. Additional segmentation tests have been performed introducing in the processing pipeline an intermediate manipulation step devoted to the extraction of textural features, following the approach outlined in section III-2.2. More precisely a Gabor filtering stage is executed to enrich the vector of features associated with the input image, vector that will be fed as input to the following K-means stage.

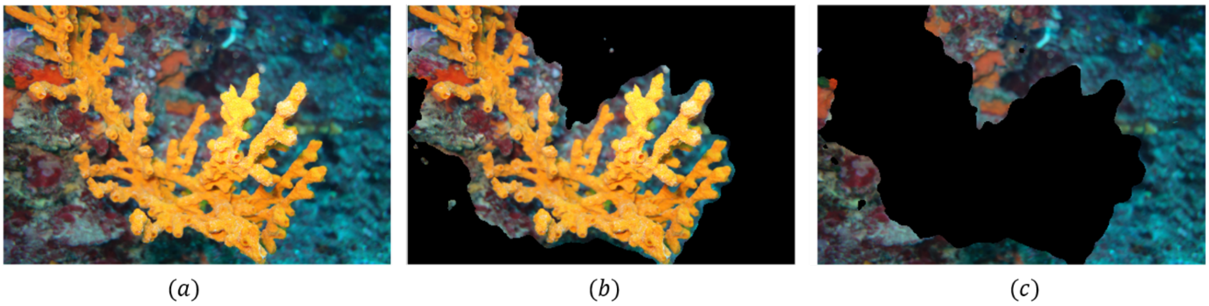

*Figure 19. K-means clustering (two classes) of Gabor features applied to an erect dendritic sponge image: (a) input image; (b) cluster I; (c) cluster II.*

Through a visual assessment of the output result (see Figure 19) it is clear that the straight clustering of Gabor textural features in the processing pipeline is not satisfactory for the underwater benthic segmentation task. The separation of the represented objects is strongly affected by the environmental conditions. First of all, light coming from sources located at varying distances from the camera suffers from different intensity decreases due to absorption. In the underwater scenario this may lead to huge illumination unbalances between background and foreground planes. Secondly, multi-source scattering affects the visibility introducing an unpredictable haze layer in the captured data and eventually reducing the signal to noise ratio. Finally, the irregularity in the visual appearance of the objects located within the surveyed scene (overlapping benthic specimens, fishes and particles temporarily present in the field of view) contributes in making the textural perception spatially incoherent, chaotic and not trivially separable.

Gabor texture features gained large popularity within the scientific community due to their striking performance in mimicking the perceptual behavior of the human vision system. On the other hand it is undisputable that in the underwater domain many factors emerge and combine to affect their discriminative power. Future effort will be devoted to experiments oriented to address an image enhancement goal, introduced within the preliminary signal processing stages of the segmentation pipeline. In no case the implemented procedure will substitute the human expertise in its decision making role. Instead, it will represent a tool providing supporting suggestions to steer the recognition task.

## 6. Seafloor fauna detection and counting

The algorithm developed for the seafloor fauna detection and counting has been designed and developed using MATLAB from MathWorks® (version R2019b). The video dataset available for the development and testing of the algorithms has been provided by the partner CNR-IRBIM, consisting of several annotated videos acquired through various campaigns in 2015 and 2016 and collected at different stations in the Adriatic Sea.

### 6.1. Background and requirements

The aim is to identify and count the number of Nephrops burrow systems falling within a fixed field of view along transects of known length. Counts of burrow systems are converted into densities at each station using the width of view and the length of the tow. Each system is assumed to represent one adult Nephrops with occupancy considered to be 100%. Overall abundance is estimated by raising the mean density to the appropriate strata area or using geostatistical methods. Total survey abundance, variance, and confidence limits are then calculated [22].

A screenshot from one of the videos is shown in Figure 20. These selected videos were 1 minute long.

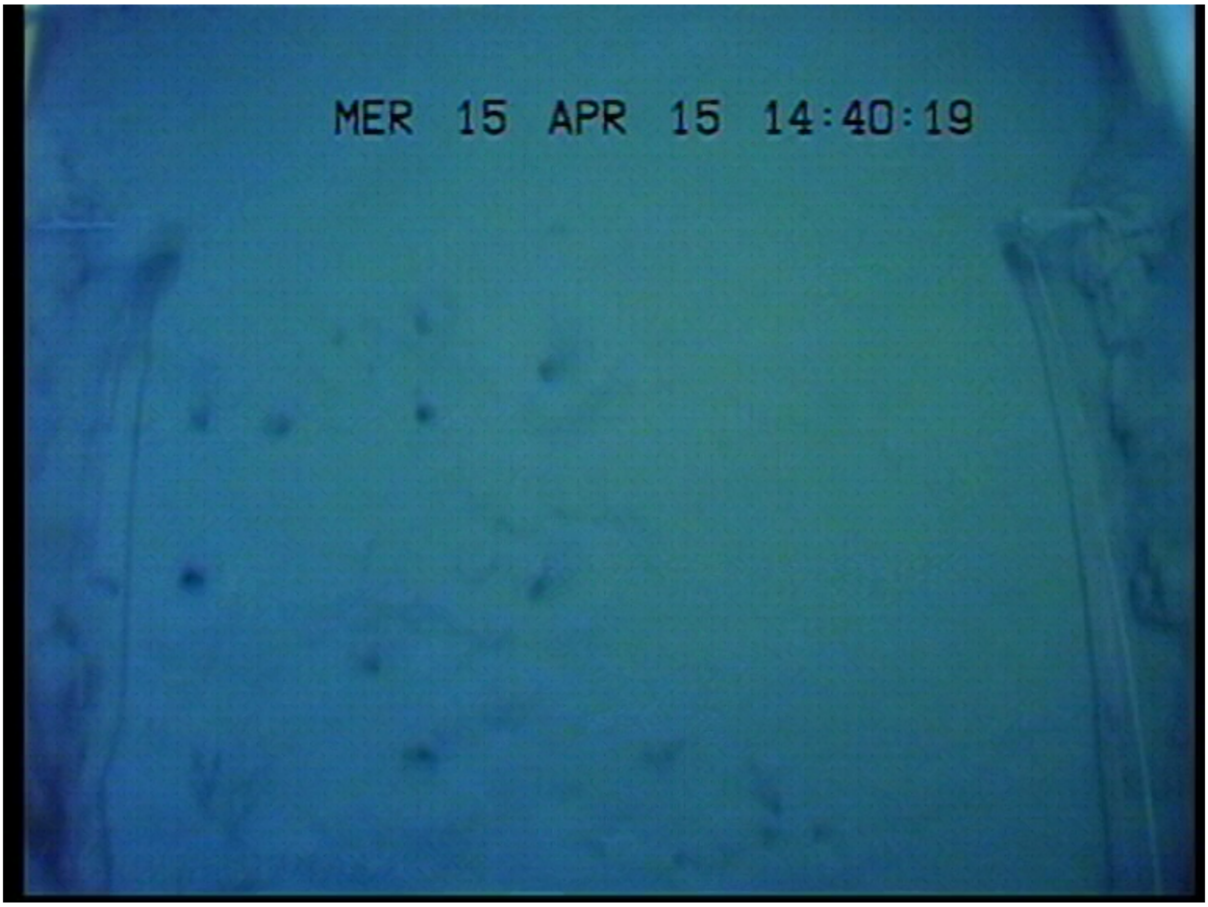

*Figure 20. Screenshot from a video acquired for the Nephrops burrows detection campaigns.*

The provided annotation consists of a Microsoft® Excel table with one row per second, linked with the observation note (e.g. “1 system left-centre + 1 collapsed right”), and the burrow count for that second, i.e. how many burrow systems in that second.

Following the extensive studies, since the early 2010s, in the ICES Working Group, the definition and characterising “signatures” of the Nephrops burrows have been outlined. For instance the appearance, the shape, and other significative features have been identified; in the following Figure 21 a sample of these is shown.

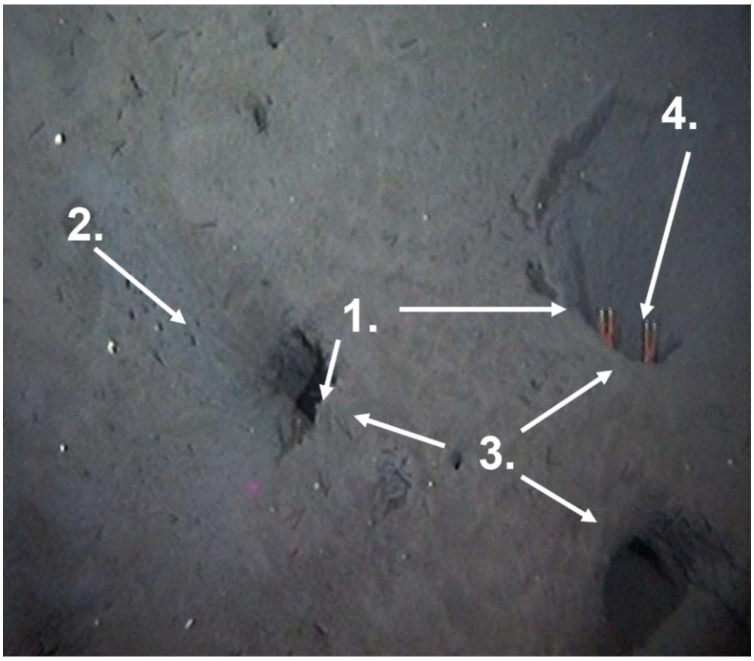

*Figure 21. Significative signatures of a Nephrops burrow system.*

In the figure, the numbered areas show the following features:

5. Crescentiform entrance of the burrow;
6. Sediment ejecta and radial scrapings around the entrance. Claw or pereiopod indents. "Drive-way"
7. Single to multiple entrances, focusing on an apparent "raised" centrum
8. Nephrops presence

Moreover, some high-level guidelines have been suggested to allow for a more standardised classification by the various ICES Working Groups experiences [22]. These guidelines were helpful in the design of the algorithm to develop a method that was as close as possible to the procedures followed by the experts in their manual (i.e. visual) efforts. The main guidelines are as follows:

- Only count systems or parts of a system that cross an imaginary line just off the bottom of the screen.
- Include an entrance to a burrow if part of the shadow is still within sight as it crosses the line.
- Look for groups of similarly sized entrances radiating from a centrum, then look for Nephrops' signatures.
- In poor visibility conditions, distinguishing the signatures will be more challenging; due to the low contrast, hemispherical entrances may appear as dark circular entrances. The signatures will appear less clear, but the ejected sediments and the disposition of the inlets will be the primary indicators.
- In the absence of Nephrops signatures, dismiss:
    - vertical holes;
    - flat holes with curved scrapings, sediment stacked in mounds.
- If in doubt, leave it out.

- Distance covered whilst the view is obscured by cloud and lifting needs to be discounted.
- Count and record in seconds, only for the period the sledge is moving.

## 6.2. The algorithm and the GUI

Following this and the meetings with experts who manually and visually classify the video, a tool based on developed algorithms and usable through a graphical user interface (GUI) has been designed to visualise better and test the automatic burrow detection tool. In the following Figure 22, the GUI is shown upon its loading.

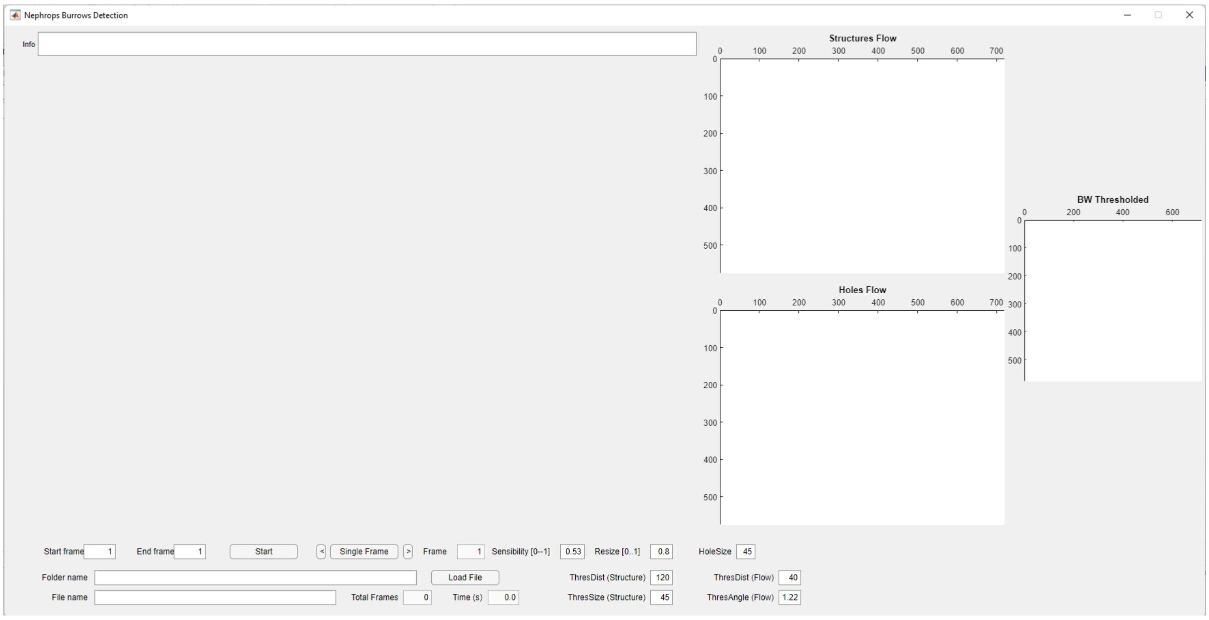

Start frame 1
End frame 1
Frame 1
Sensibility [0--1] 0.53
Resize [0..1] 0.8
HoleSize 45
Folder name
ThresDist (Structure) 120
ThresDist (Flow) 40
File name
Total Frames 0
Time (s) 0.0
ThresSize (Structure) 45
ThresAngle (Flow) 1.22

*Figure 22. The Graphical User Interface developed for the Nephrops burrow detection tool.*

The GUI is divided into three main areas: the left-centre panel will be filled by the images to be processed; in the centre-right and right panels, the graphs showing information will be represented; while the bottom part of the interface contains the buttons and fields used for controlling the tool (e.g. the button for loading a video file, for automatically processing a range of frames, for processing a single frame or the next one…), for viewing the video/frame information (e.g. video length, current frame number and time within the video…), as well as for setting the processing parameters (e.g. sensibility of the processing filters, the minimum size of holes, tracking and thresholding parameters for the geometries).

The first step to perform is selecting and loading the video to be analysed. An apparent problem can be seen as soon as the video is loaded due to the interlaced video acquired from TV recording (Figure 23). Thus, the first preprocessing step was to remove this interlacement and improve the single frame appearance. The difference can be seen in the following Figure 24 from the same frame after being loaded (left), and once it has been preprocessed, and ready for the beginning of processing (right).

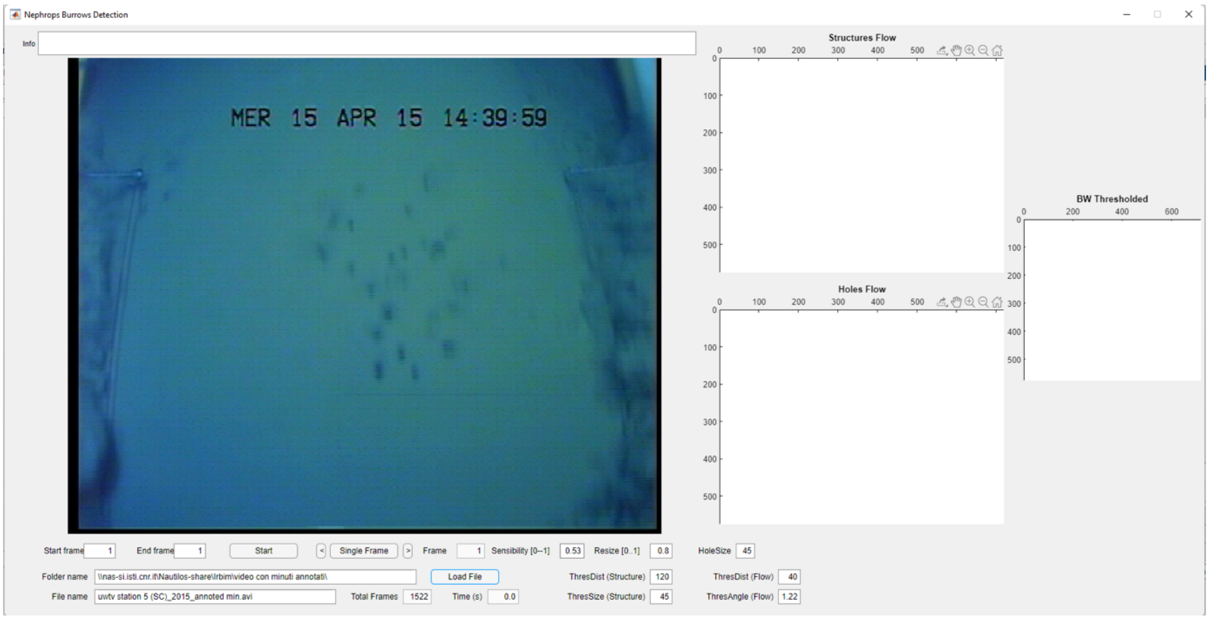

Nephrops Burrows Detection

Info

Start frame 1 End frame 1 Start < Single Frame > Frame 1 Sensibility [0--1] 0.53 Resize [0..1] 0.8 HoleSize 45

Folder name \\nas-si.isti.cnr.it\Nautilos-share\Irbim\video con minuti annotati\ Load File ThresDist (Structure) 120 ThresDist (Flow) 40

File name uwtv station 5 (SC)_2015_annoted min.avi Total Frames 1522 Time (s) 0.0 ThresSize (Structure) 45 ThresAngle (Flow) 1.22

*Figure 23. Loaded video file from GUI, showing first original frame.*

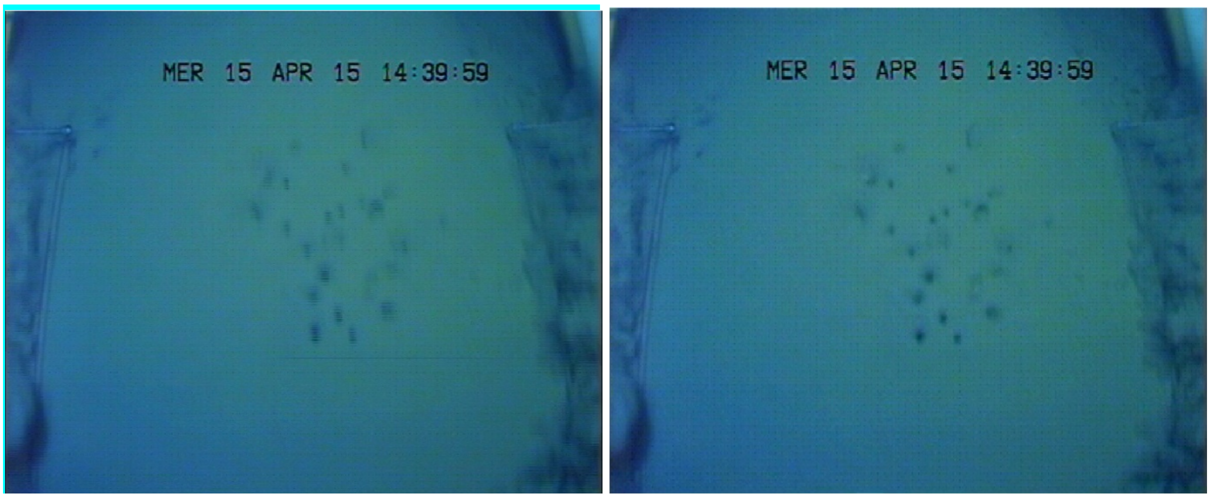

*Figure 24. Example of an original frame of the video (left) and after pre-processing (right).*

The general processing steps foresee two different analysis phases: only for the first frame the holes identification and selection, followed by the analysis and identification of the structures; on the subsequent frames, these first steps are repeated, but then the optical flow is used to understand and create connections between the identified holes and mainly among the identified structures. The processing flow diagram is shown in Figure 25.

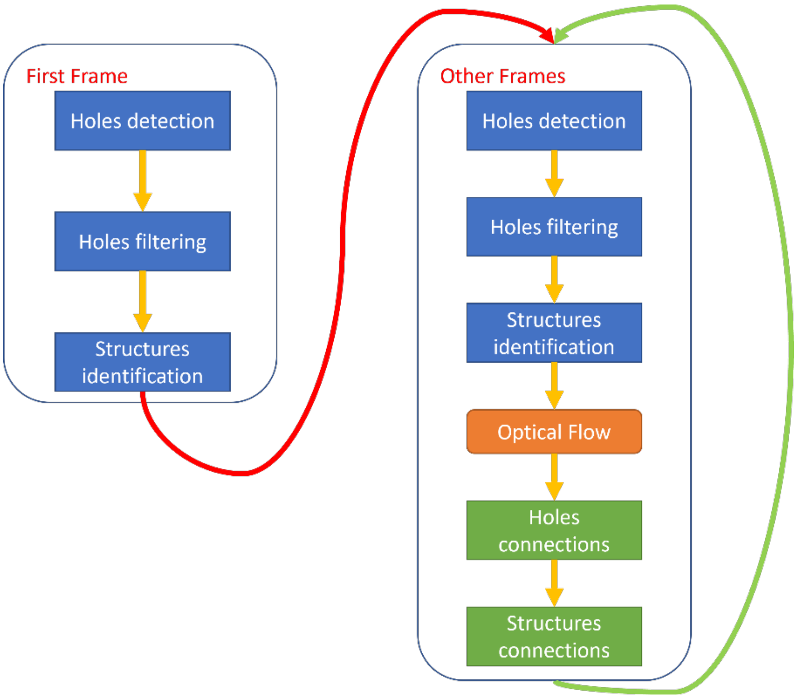

*Figure 25. Flow diagram of the Nephrops burrow algorithm.*

As a first processing step, holes are recognised through the identification of connected regions in the negative image using adaptive thresholding. The result of this processing is shown in the rightmost panel (blue/yellow coloured graph) of the GUI (see Figure 26).

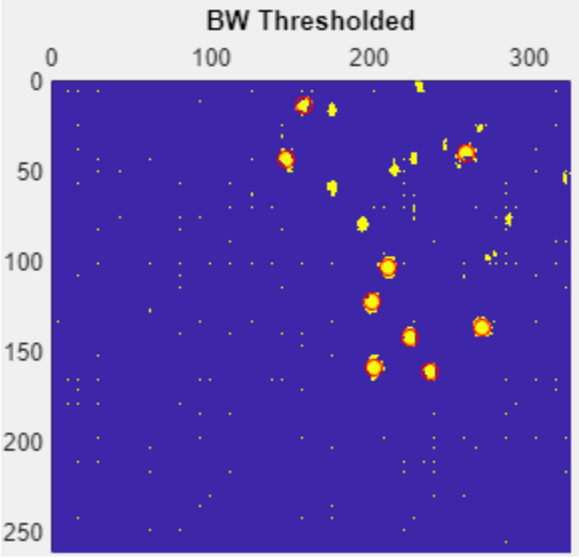

*Figure 26. Initial processing results before filtering.*

Subsequent processing steps filter over the detected holes to dismiss those below thresholds for dimension, shape, or position. Moreover, a colour histogram detects possible shadows and rejects them from the potential holes. Once the number of candidate holes is reduced, the geometric features are computed to analyse the shapes further. Features like: area, perimeter, the major axis of the area, eccentricity and circularity are extracted as well as the bounding box of each candidate hole.

Based on these parameters, rules have been defined for evaluating proximity, shape consistency, distances among holes and similarity by other geometric features. Based on these factors, structures composing a burrow system are identified. In the following Figure 27 the detection and identification of a structure, identified with its bounding box (green rectangle) and its composing holes (inside the red circles) are highlighted.

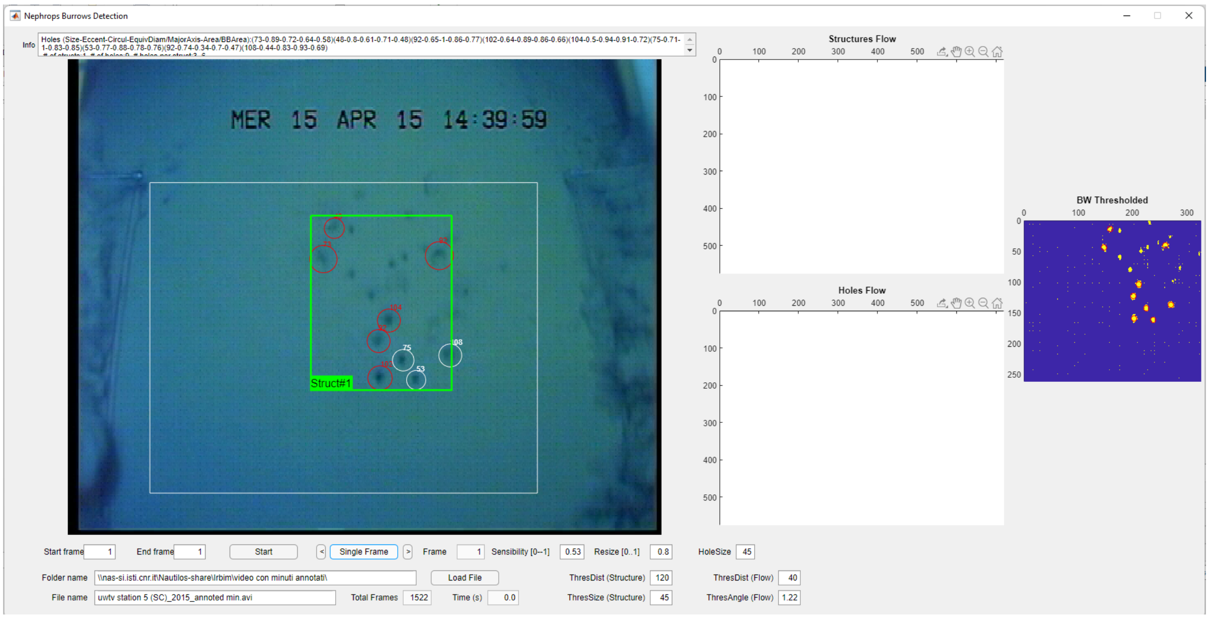

Info: Holes (Size-Eccent-Circul-EquivDiam/MajorAxis-Area/BBArea):(73-0.89-0.72-0.64-0.58)(48-0.8-0.61-0.71-0.48)(92-0.65-1-0.86-0.77)(102-0.64-0.89-0.86-0.66)(104-0.5-0.94-0.91-0.72)(75-0.71-1-0.83-0.85)(53-0.77-0.88-0.78-0.76)(92-0.74-0.34-0.7-0.47)(108-0.44-0.83-0.93-0.69)

Start frame: 1 End frame: 1 Frame: 1 Sensibility [0--1]: 0.53 Resize [0..1]: 0.8 HoleSize: 45

Folder name: \\nas-si.isti.cnr.it\Nautilos-share\Irbim\video con minuti annotati\ ThresDist (Structure): 120 ThresDist (Flow): 40

File name: uwtv station 5 (SC)_2015_annoted min.avi Total Frames: 1522 Time (s): 0.0 ThresSize (Structure): 45 ThresAngle (Flow): 1.22

*Figure 27. Detection and identification of holes (red circles) and the structure (highlighted green rectangle) composed by these holes; the holes in white circles are identified as candidate holes but dismissed and not associated with the structure.*

The figure also shows some holes (in white circles) that have been identified as candidate holes but then filtered and discarded from the identified structure, due to a missing correspondence to the structure's geometric and appearance parameters.

Another example of filtered areas is shown in the following Figure 28; here, the noise brought in the video by the cloud of sand caused by the movement of the sledge on the left side is identified and easily filtered out as a false alarm and highlighted in the large white circle. The small numbers next to the circles represent the dimension of the identified connected areas, regardless of whether they belong to a structure. Furthermore, the text box above the processing frame shows statistics and information about the holes and structures identified in the current frame.

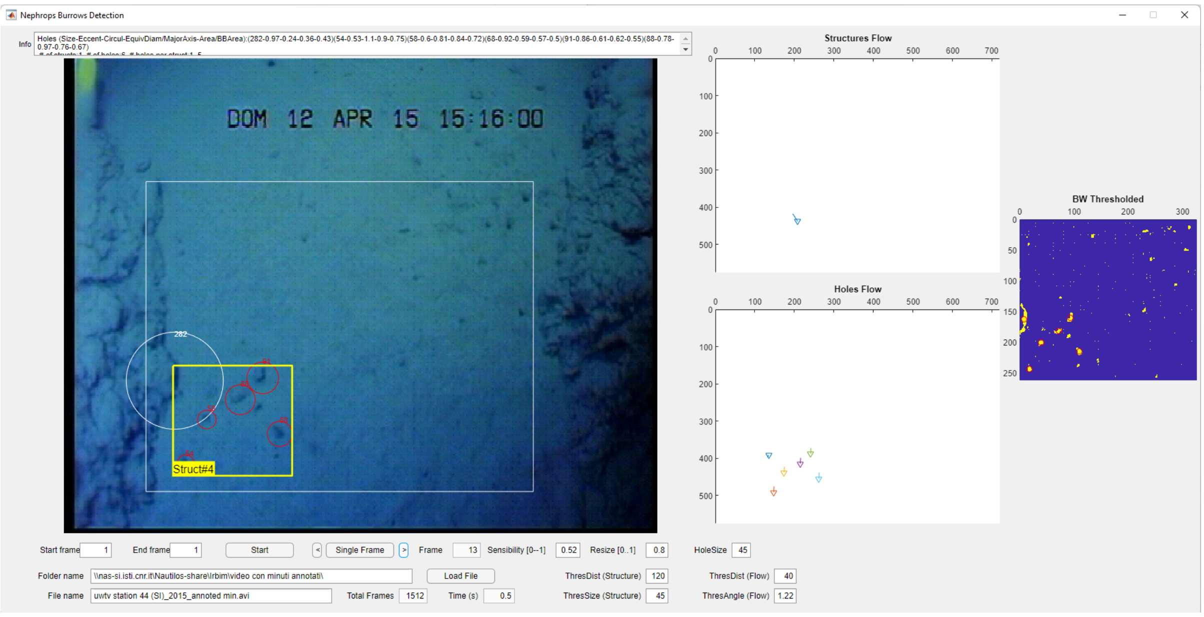

Nephrops Burrows Detection

Info: Holes (Size-Eccent-Circul-EquivDiam/MajorAxis-Area/BBArea):(282-0.97-0.24-0.36-0.43)(54-0.53-1.1-0.9-0.75)(58-0.6-0.81-0.84-0.72)(68-0.92-0.59-0.57-0.5)(91-0.86-0.61-0.62-0.55)(88-0.78-0.97-0.76-0.67)
# of structs:1, # of holes:6, # holes per struct:1, 5

Start frame 1 | End frame 1 | Start | < | Single Frame | > | Frame 13 | Sensibility [0--1] 0.52 | Resize [0..1] 0.8 | HoleSize 45

Folder name \\nas-si.isti.cnr.it\Nautilos-share\Irbim\video con minuti annotati\ | Load File | ThresDist (Structure) 120 | ThresDist (Flow) 40

File name uwtv station 44 (SI)_2015_annoted min.avi | Total Frames 1512 | Time (s) 0.5 | ThresSize (Structure) 45 | ThresAngle (Flow) 1.22

*Figure 28. Detection and identification of holes and structure (red circles, yellow rectangle) composed by these holes; the detected area in the white circle is dismissed and not associated with the structure.*

The next step, applied to all subsequent frames of the video, consists of the same detection and filtering steps as mentioned above, followed by an optical flow computation between the current frame structures and holes and the previous frame ones.

These optical flows are computed and then filtered, considering the known motion of the sledge and the geometric features of both the holes and structures. The optical flows are shown in the GUI central-right graphs (see Figure 29). A confusion matrix is computed associating holes/structures in frame $i$ and in frame $i-1$. This matrix is also important to understand whether a structure is persistent in subsequent frames or changed so that it should be identified as a new structure.

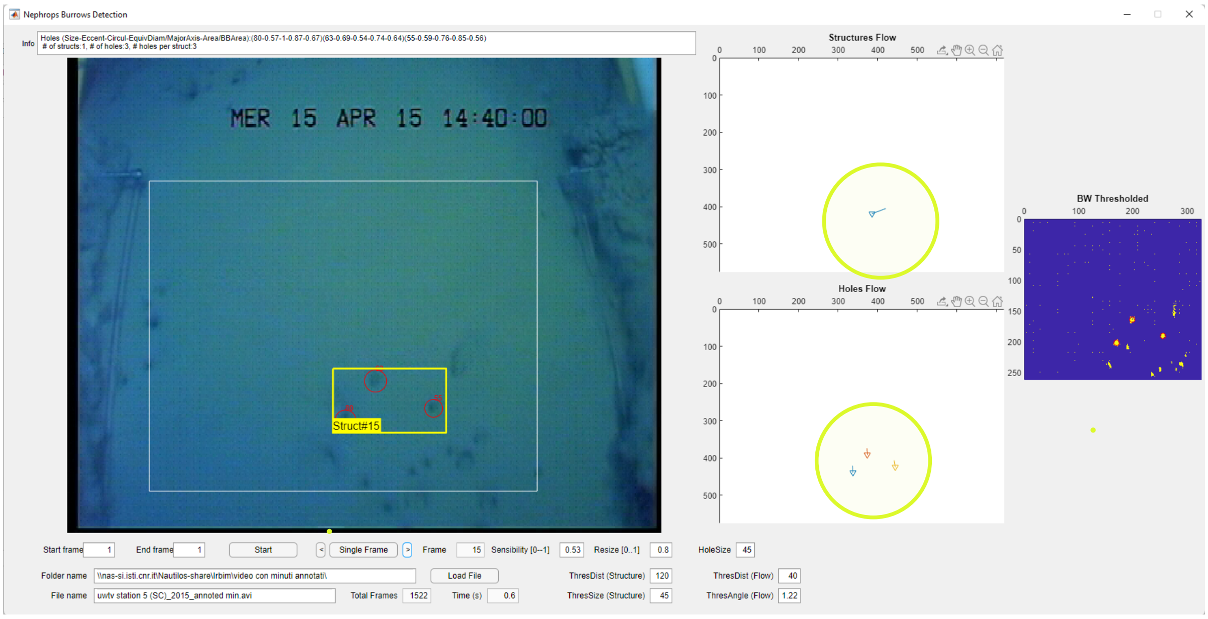

Nephrops Burrows Detection

Info: Holes (Size-Eccent-Circul-EquivDiam/MajorAxis-Area/BBArea):(80-0.57-1-0.87-0.67)(63-0.69-0.54-0.74-0.64)(55-0.59-0.76-0.85-0.56)
# of structs:1, # of holes:3, # holes per struct:3

Start frame 1 | End frame 1 | Start | < | Single Frame | > | Frame 15 | Sensibility [0--1] 0.53 | Resize [0..1] 0.8 | HoleSize 45

Folder name \\nas-si.isti.cnr.it\Nautilos-share\Irbim\video con minuti annotati\ | Load File | ThresDist (Structure) 120 | ThresDist (Flow) 40

File name uwtv station 5 (SC)_2015_annoted min.avi | Total Frames 1522 | Time (s) 0.6 | ThresSize (Structure) 45 | ThresAngle (Flow) 1.22

*Figure 29. Highlight of the holes (lower yellow circle) and structures (upper yellow-circle) optical flows between the current frame and previous one.*

More than one structure can be present on the same frame, and the algorithm is developed to keep track and count them separately. In Figure 30 an example with two different structures was detected, while in Figure 31 an instance with 3 separate structures on the same frame is shown. In both these situations, it can be seen that the tracking of the structures, shown in the upper-right-centre panel, is maintained. For the 2 structures case, the upper one (#8) is not present in the tracking because it is a newly identified structure and thus coloured in red.

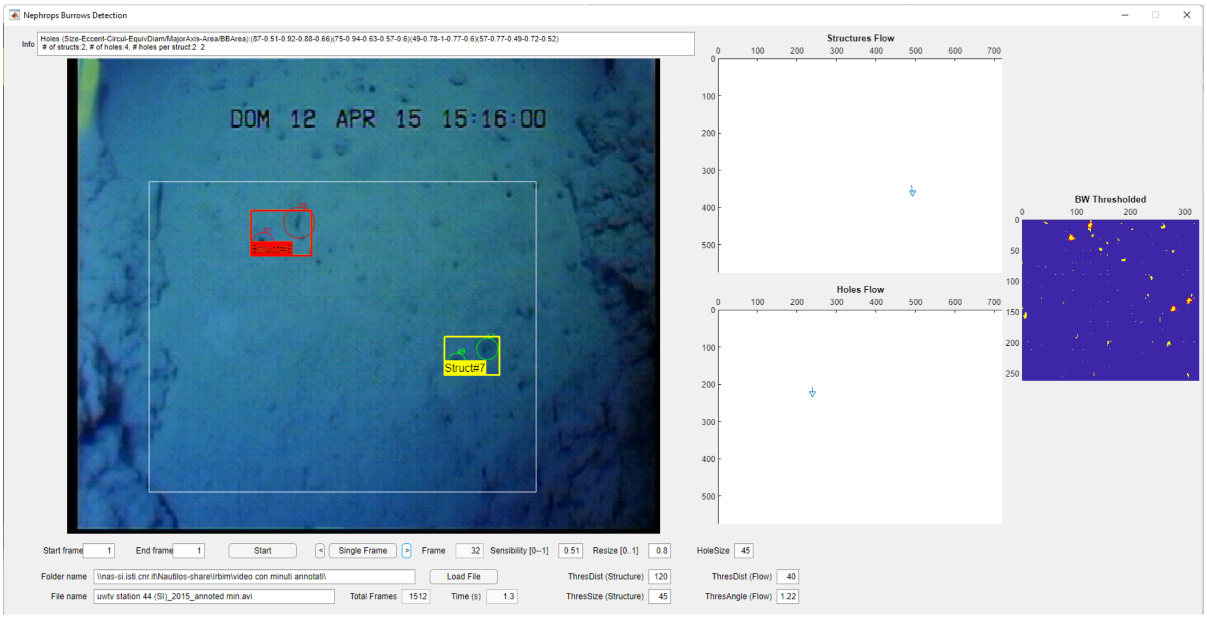
Nephrops Burrows Detection

Info: Holes (Size-Eccent-Circul-EquivDiam/MajorAxis-Area/BBArea):(87-0.51-0.92-0.88-0.66)(75-0.94-0.63-0.57-0.6)(49-0.78-1-0.77-0.6)(57-0.77-0.49-0.72-0.52)
# of structs:2, # of holes:4, # holes per struct:2  2

Start frame 1 · End frame 1 · Start · < Single Frame > · Frame 32 · Sensibility [0--1] 0.51 · Resize [0..1] 0.8 · HoleSize 45

Folder name \\nas-si.isti.cnr.it\Nautilos-share\Irbim\video con minuti annotati\ · Load File · ThresDist (Structure) 120 · ThresDist (Flow) 40

File name uwtv station 44 (SI)_2015_annoted min.avi · Total Frames 1512 · Time (s) 1.3 · ThresSize (Structure) 45 · ThresAngle (Flow) 1.22

Figure 30. Example of multiple structures (2) detected.

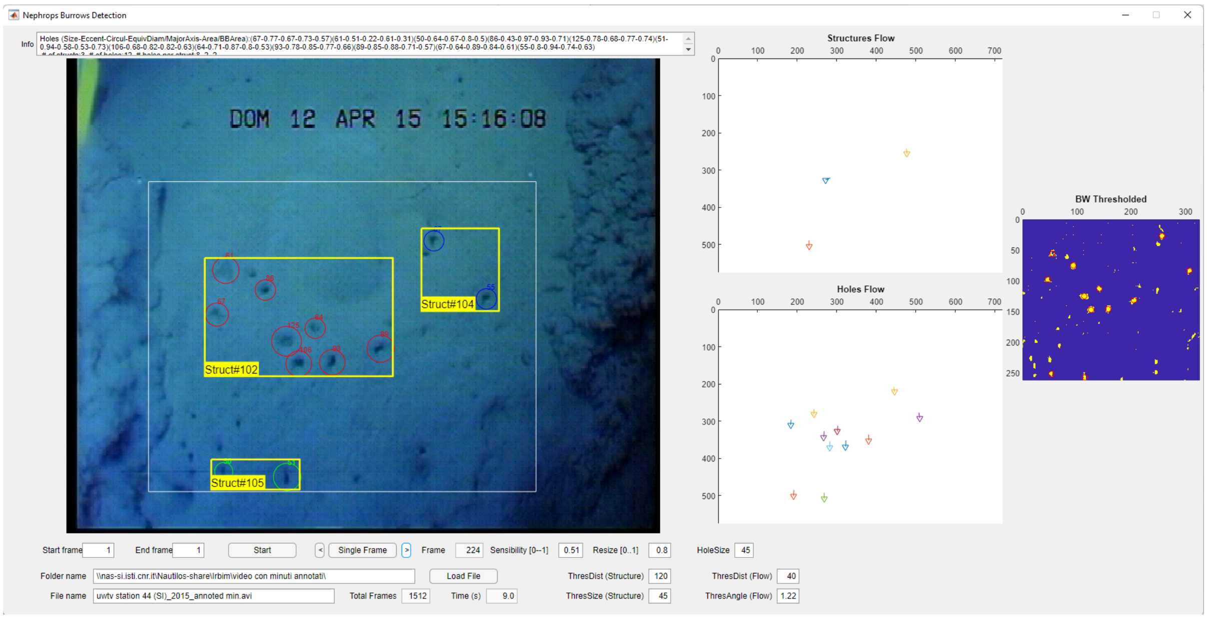
Nephrops Burrows Detection

Info: Holes (Size-Eccent-Circul-EquivDiam/MajorAxis-Area/BBArea):(67-0.77-0.67-0.73-0.57)(61-0.51-0.22-0.61-0.31)(50-0.64-0.67-0.8-0.5)(86-0.43-0.97-0.93-0.71)(125-0.78-0.68-0.77-0.74)(51-0.94-0.58-0.53-0.73)(106-0.68-0.82-0.82-0.63)(64-0.71-0.87-0.8-0.53)(93-0.78-0.85-0.77-0.66)(89-0.85-0.88-0.71-0.57)(67-0.64-0.89-0.84-0.61)(55-0.8-0.94-0.74-0.63)
# of structs:3, # of holes:12, # holes per struct:8  2  2

Start frame 1 · End frame 1 · Start · < Single Frame > · Frame 224 · Sensibility [0--1] 0.51 · Resize [0..1] 0.8 · HoleSize 45

Folder name \\nas-si.isti.cnr.it\Nautilos-share\Irbim\video con minuti annotati\ · Load File · ThresDist (Structure) 120 · ThresDist (Flow) 40

File name uwtv station 44 (SI)_2015_annoted min.avi · Total Frames 1512 · Time (s) 9.0 · ThresSize (Structure) 45 · ThresAngle (Flow) 1.22

Figure 31. Another example with three different structures identified.

In this last example, the structures numbered #102 (with holes in red) and #104 (with holes in blue) are identified as different and separated ones: this is due to differences in the geometry of the two groups of composing holes, as well as due to distances between the composing holes.

On the other hand, the following Figure 32 shows a different example of multiple structures detected where two of them are overlapped. Structure #99 (with red holes) and #101 (with blue holes) are identified as different structures with holes belonging to each separate system due to the various geometric features of the holes themselves and characterising the two systems.

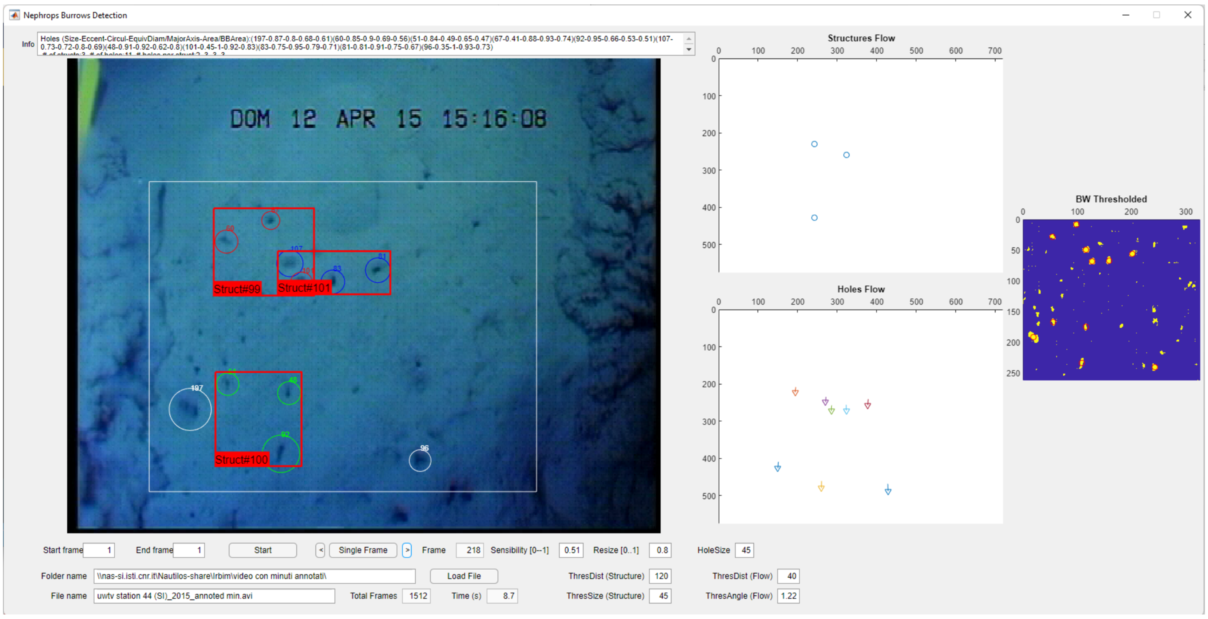

Info: Holes (Size-Eccent-Circul-EquivDiam/MajorAxis-Area/BBArea):(197-0.87-0.8-0.68-0.61)(60-0.85-0.9-0.69-0.56)(51-0.84-0.49-0.65-0.47)(67-0.41-0.88-0.93-0.74)(92-0.95-0.66-0.53-0.51)(107-0.73-0.72-0.8-0.69)(48-0.91-0.92-0.62-0.8)(101-0.45-1-0.92-0.83)(83-0.75-0.95-0.79-0.71)(81-0.81-0.91-0.75-0.67)(96-0.35-1-0.93-0.73)
# of structs:3 # of holes:11 # holes per struct:2 3 3 3

Start frame 1 End frame 1 Frame 218 Sensibility [0--1] 0.51 Resize [0..1] 0.8 HoleSize 45

Folder name \\nas-si.isti.cnr.it\Nautilos-share\Irbim\video con minuti annotati\ ThresDist (Structure) 120 ThresDist (Flow) 40

File name uwtv station 44 (SI)_2015_annoted min.avi Total Frames 1512 Time (s) 8.7 ThresSize (Structure) 45 ThresAngle (Flow) 1.22

*Figure 32. Example of multiple and overlapping structures identified.*

The tool is then complete, but further improvements will be applied following extended testing and feedback from end-users and other videos even acquired from entirely different environments and situations.

# V. Conclusions

This deliverable represents an accompanying report for the automatic image tools designed and developed as the main activities of Task 8.5 within Work Package 8 in NAUTILOS. The report describes the work performed, starting from the identification, analysis and definition of diverse environmental domains and connected problems performed with the support of NAUTILOS partners and based on their expertise. As a part of the analysis, the state of the art of the literature relating to the various problems was studied. Since both the environmental domains and the problems are very different from each other, the state of the art needed to be presented in a very different way and at very different levels.

The algorithms chosen for the automatic imagery processing objective, have been described and presented with the developed tools for performing analysis and testing. Considering the diversity of the requirements and categorization, the process of improving these algorithms will proceed through continuous feedbacks from experts and end-users, as part of Task 9.5 activities.

Whenever possible, the developed software code will be integrated with the NAUTILOS data infrastructure and made freely available through open access platforms.

Furthermore, updated and improved versions of the various algorithms will be provided. Multidisciplinary dissemination will not be ignored, and the objectives of applied scientific communication will also be pursued through conferences or publications in dedicated journals, following a path that has already proven prolific and promising.

# VI. Bibliography

[1] OSI SAF, *Full resolution L2P AVHRR Sea Surface Temperature MetaGRanules (GHRSST) - Metop,* EUMETSAT SAF on Ocean and Sea Ice, 2011.

[2] NASA/JPL, *GHRSST Level 2P Global Sea Surface Skin Temperature from the Moderate Resolution Imaging Spectroradiometer (MODIS) on the NASA Aqua satellite (GDS2),* NASA Physical Oceanography DAAC, 2020.

[3] FAO, «The State of World Fisheries and Aquaculture 2018 - Meeting the sustainable development goals,» Roma, 2018.

[4] R. Varela, I. Álvarez, F. Santos, M. T. de Castro e M. Gómez-Gesteira, «Has upwelling strengthened along worldwide coasts over 1982-2010?,» *Scientific Reports,* vol. 5, p. 10016, 2015.

[5] J. Janeiro, *Development of an operational tool for oil spill forecast: Application to oil exposed regions,* University of Algarve, 2014.

[6] F. P. Chavez e M. Messié, «A comparison of Eastern Boundary Upwelling Ecosystems,» *Progress in Oceanography,* vol. 83, n. 1, pp. 80-96, 2009.

[7] V. AA, «EMODnet Recommended Operating Guidelines,» 2007. [Online]. Available: https://www.emodnet-seabedhabitats.eu/resources/recommended-operating-guidelines/.

[8] R. Nock e F. Nielsen, «Statistical Region Merging,» *IEEE transactions on pattern analysis and machine intelligence,* vol. 26, n. 11, pp. 1452-8, 2004.

[9] A. C. Bovik, M. Clark e W. S. Geisler, «Multichannel Texture Analysis Using Localized Spatial Filters,» *IEEE Transactions On Pattern Analysis And Machine Intelligence,* vol. 12, n. 1, pp. 55-73, 1990.

[10] M. Johnson-Roberson, S. Kumar e S. Williams, «Segmentation and Classification of Coral for Oceanographic Surveys: A Semi-Supervised Machine Learning Approach,» in *OCEANS 2006 - Asia Pacific*, Singapore, 2006.

[11] A. K. Jain e F. Farrokhnia, «Unsupervised texture segmentation using Gabor filters,» *Pattern Recognition,* vol. 24, n. 12, pp. 1167-1186, 1991.

[12] L. Holthuis, «Norway lobster (Nephrops norvegicus),» [Online]. Available: http://species-identification.org/species.php?species_group=lobsters&id=107.

[13] EU Network of Excellence 'Marine Biodiversity and Ecosystem Functioning' (MarBEF), «Nephrops norvegicus,» [Online]. Available: https://www.marinespecies.org/aphia.php?p=taxdetails&id=107254#links.

[14] J. Aguzzi, N. Bahamon, J. Doyle, C. Lordan, I. D. Tuck, M. Chiarini, M. Martinelli e J. B. Company, «Burrow emergence rhythms of Nephrops norvegicus by UWTV and surveying biases,» *Scientific Reports,* vol. 11, n. 0, p. 5797, 2021.

[15] H. Dobby, J. Doyle, J. Jónasson, P. Jonsson, A. Leocádio, C. Lordan, A. Weetman e a. K. Wieland, «ICES Survey Protocols – Manual for Nephrops Underwater TV Surveys, coordinated under ICES Working Group on Nephrops Surveys (WGNEPS),» ICES, 2021.

[16] R. J. A. Atkinson e A. C. Taylor, «Aspects of the physiology, biology and ecology of thalassinidean shrimps in relation to their burrow environment.,» *Oceanography and Marine Biology,* pp. 183-220, 2005.

[17] A. Naseer, E. N. Baro, S. D. Khan e Y. V. Gordillo, «Automatic Detection of Nephrops norvegicus Burrows in Underwater Images Using Deep Learning,» in *2020 Global Conference on Wireless and Optical Technologies (GCWOT)*, Malaga, Spain, 2021.

[18] O. Papini, «A tool for the temporal analysis of sea surface temperature maps,» 2021.

[19] M. Reggiannini, J. Janeiro, F. Martins, O. Papini e G. Pieri, «Mesoscale Patterns Identification Through SST Image Processing,» in *Proceedings of the 2nd International Conference on Robotics, Computer Vision and Intelligent Systems — ROBOVIS*, 2021.

[20] O. Papini, M. Reggiannini e G. Pieri, «SST Image Processing for Mesoscale Patterns Identification,» *Engineering Proceedings,* vol. 8, p. 5, 2021.

[21] O. Papini, «SpaghettiData and SpaghettiPlot: two Python classes for analysing and visualising SST trends,» 2022.

[22] R. Masefield, K. Vanstaen, A. M. Leocadio, C. Barrett, N. Edmonds, V. Laptikhovsky, M. Whybrow, N. Needham, H. Nutt e M. Rijkeboer, «Farn Deeps Nephrops Grounds (FU6) 2016 UWTV Survey Report.,» 2016.

# VII. Appendix 1: References and Related Documents

| ID | Reference or Related Document | Source or Link/Location |
|---|---|---|
| 1 | *NAUTILOS Grant Agreement* | *NAUTILOS OwnCloud* |